J. Fluid Mech. (1998), *vol.* 360, *pp.* 141–178. Printed in the United Kingdom

Strongly nonlinear convection cells in a rapidly rotating fluid layer: the tilted f-plane

By KEITH JULIEN[1, 2] AND EDGAR KNOBLOCH[3, 4]

[1] National Center for Atmospheric Research, Boulder, CO 80307, USA

[2] Department of Applied Mathematics, University of Colorado, Boulder, CO 80309, USA

[3] JILA, University of Colorado, Boulder, CO 80309, USA

[4] Department of Physics, University of California, Berkeley, CA 94720, USA

(Received 29 April 1997 and in revised form 18 November 1997)

Investigation of the linear stability problem for rapidly rotating convection on an f-plane has revealed the existence of two distinct scales in the vertical structure of the critical eigenfunctions: a small length scale whose vertical wavenumber k_z is comparable with the large horizontal wavenumber $k_\perp$ selected at onset, and a large-scale modulation which forms an envelope on the order of the layer depth d. The small-scale structure in the vertical results from a geostrophic balance imposed by the Taylor–Proudman constraint. This primary balance forces rotational alignment and confines fluid motions to planes perpendicular to the rotation axis. For convective transport in the vertical this constraint must be relaxed. This is achieved by molecular dissipation which allows weak upward (downward) spiralling of hot (cold) fluid elements across the Taylor–Proudman planes and results in a large-scale vertical modulation of the Taylor columns.

In the limit of fast rotation (i.e. large Taylor number) a multiple-scales analysis leads to the determination of a critical Rayleigh number as a function of wavenumber, roll orientation and the tilt angle of the f-plane. The corresponding critical eigenfunction represents the core solution; matching to passive Ekman boundary layers is required for a complete solution satisfying boundary conditions.

An extension of this analysis, introduced by Bassom & Zhang (1994), is used to describe strongly nonlinear two-dimensional convection, characterized by significant departures of the mean thermal field from its conduction profile. The analysis requires the solution of a nonlinear eigenvalue problem for the Nusselt number (for steady convection) and the Nusselt number and oscillation frequency (for the overstable problem). The solutions of this problem are used to calculate horizontal and vertical heat fluxes, as well as Reynolds stresses, as functions of both the latitude and roll orientation in the horizontal, and these are used to calculate *self-consistently* north–south and east–west mean flows. These analytical predictions are in good agreement with the results of three-dimensional simulations reported by Hathaway & Somerville (1983).

1. Introduction

Convective heat transport plays a major role in the energy balance of the atmosphere and the oceans. This fact has provided an important impetus for the study of rotating turbulence and specifically rotating turbulent convection. Such studies have

typically employed numerical simulations of the primitive equations (Hathaway & Somerville 1983; Julien *et al.* 1996) or laboratory experiments (Ohlsen, Hart & Kittelman 1995). Analytical theories, such as weakly nonlinear expansions, are usually of little relevance in the atmospheric context. Consequently there are few theoretical predictions that can be tested against or compared with the simulations and experiments. In this paper we report on a theoretical investigation of two-dimensional rotating convection in the high-Taylor-number regime which yields analytical but fully nonlinear predictions for a number of quantities of importance in atmospheric science. Among these we mention horizontal heat fluxes, the Reynolds stress tensor and horizontal mean flows. We formulate the problem at arbitrary latitude, and suppose the fluid to be confined between two locally horizontal plane boundaries held at fixed temperatures (the lower being hotter), but otherwise unbounded in the horizontal. We make the simple observation that unless the initial convective rolls are oriented in the north–south direction the presence of the strong Coriolis force generates small scales in the locally vertical direction. These scales are comparable to the horizontal scales which are also small in this limit. We examine the consequences of the presence of these small scales on the transport properties of the convection, and compare a number of measures of transport effectiveness (some of which we have listed above) for fully nonlinear solutions with and without these small scales. We find that the former are indeed more effective at transport (both heat and momentum), in the sense that the horizontal mean flows generated are substantially larger as are the heat fluxes. Our analytical results are in surprisingly good agreement with the three-dimensional simulations of Hathaway & Somerville (1983) even though our asymptotic expansion is fundamentally two-dimensional. We believe that our results have important implications for mixing length theories of convective transport when these are used at normal latitudes, essentially because the rapid rotation introduces a new length scale into the theory, in addition to the vertical scale height.

To our knowledge there exists no published discussion of the small vertical scales generated by the Taylor-Proudman constraint, although Hathaway, Gilman & Toomre (1979) constructed two-scale normal modes of the correct form in their study of rotating convection without diffusion. Subsequent work of Hathaway, Toomre & Gilman (1980) with diffusion focused on the effects of an imposed thermal wind, and not on the structure of the eigenfunctions. Our work can be viewed as an extension of these linear stability investigations and relies in its incarnation as a nonlinear eigenvalue problem on recent work by Bassom & Zhang (1994). This approach has much in common with the philosophy espoused by Baker & Spiegel (1975) in connection with their study of single-mode rotating convection. In fact our technique can be used as an asymptotic justification of the single-mode approach for two-dimensional planforms, i.e. rolls.

In the next section we discuss some simple properties of the basic equations of Boussinesq convection on the f-plane. In §3 we describe numerical solutions of the linear stability problem to motivate our interest in the small vertical scales mentioned above. We then describe a simple two-scale analysis which captures the two-scale structure of the critical eigenfunction. In §4 we describe the asymptotic expansion which leads to a nonlinear eigenvalue problem for the Nusselt number (the eigenvalue) and the mean temperature profile (the eigenfunction). This solution represents the state of the fluid in the bulk; the solution must be completed by matching this solution through boundary layers at the top and bottom to the imposed boundary conditions. This process is summarized in Appendix A; the required Ekman boundary layers are found to be passive and hence unimportant in this type of problem. In particular they

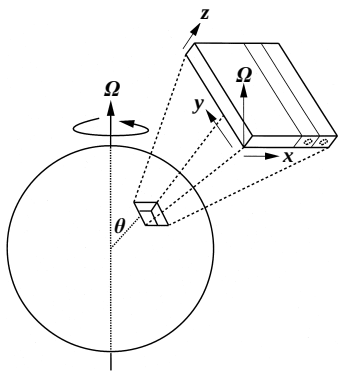

FIGURE 1. The geometry of the f-plane, illustrating north–south oriented rolls.

have no effect on the bulk eigenmode or the critical Rayleigh number. However, they do produce the spiralling in the mean-flow fields observed in numerical simulations (Brummell, Hurlburt & Toomre 1998; Julien *et al.* 1997) and in extrapolations from linear stability theory (Julien *et al.* 1997). In §5 we turn to overstable convection present for sufficiently small Prandtl numbers. The nonlinear eigenvalue problem is now complex and yields the nonlinear oscillation frequency in addition to the (time-averaged) Nusselt number. Finally in §6 we compute the transport properties of our solutions as functions of latitude and orientation in the horizontal, and compare the results for north–south and east–west rolls not only with each other but also with the numerical simulations of Hathaway & Somerville (1983). The paper concludes with a brief discussion of the implication of our results.

2. Governing equations

The dimensionless Boussinesq equations describing convection in a plane horizontal layer at latitude $90^\circ - \vartheta$ are

$$\frac{1}{\sigma}\frac{\mathrm{D}\boldsymbol{u}}{\mathrm{D}t} + Ta^{1/2}\hat{\boldsymbol{\Omega}} \times \boldsymbol{u} = -\nabla p + RaT\hat{\boldsymbol{z}} + \nabla^2\boldsymbol{u}, \tag{2.1}$$

$$\frac{\mathrm{D}T}{\mathrm{D}t} = \nabla^2 T, \tag{2.2}$$

$$\nabla \cdot \boldsymbol{u} = 0, \tag{2.3}$$

where $\boldsymbol{u} = (u, v, w)$ is the velocity field in Cartesian coordinates (x, y, z) with x eastwards, y northwards, and z vertically upwards. The symbols T and p denote the temperature and pressure, while $f_0 = 2|\boldsymbol{\Omega}|$ is the planetary rotation constant with the unit rotation vector $\hat{\boldsymbol{\Omega}} = (0, \sin\vartheta, \cos\vartheta)$, where ϑ is the colatitude. The geometry is illustrated in figure 1. The equations have been non-dimensionalized with respect to the thermal diffusion time in the vertical. The resulting dimensionless parameters

$$Ta = \frac{f_0^2 d^4}{\nu^2}, \quad Ra = \frac{g\alpha\Delta T d^3}{\nu\kappa}, \quad \sigma = \frac{\nu}{\kappa}, \tag{2.4}$$

are the Taylor, Rayleigh and Prandtl numbers, respectively.

We shall find, *a posteriori*, that the primitive variable formulation leads to ambiguities in the interpretation of the asymptotic method used. We thus favour a

streamfunction formulation from the outset, and write

$$\boldsymbol{u} = \nabla \times \phi\hat{\boldsymbol{z}} + \nabla \times \nabla \times \psi\hat{\boldsymbol{z}}. \tag{2.5}$$

Thus

$$\boldsymbol{u} = \begin{pmatrix} \partial_y\phi & + & \partial_x\partial_z\psi \\ -\partial_x\phi & + & \partial_y\partial_z\psi \\ & - & \nabla_\perp^2\psi \end{pmatrix}, \qquad \boldsymbol{\omega} = \begin{pmatrix} \partial_x\partial_z\phi & - & \nabla^2\partial_y\psi \\ \partial_y\partial_z\phi & + & \nabla^2\partial_x\psi \\ & - & \nabla_\perp^2\phi \end{pmatrix}, \tag{2.6}$$

where $\boldsymbol{\omega} \equiv \nabla \times \boldsymbol{u}$ is the vorticity. Partials with subscripts denote differentiation with respect to that variable, $\partial_x \equiv \partial/\partial x$, and $\nabla_\perp^2 \equiv \partial_{xx} + \partial_{yy}$ is the horizontal Laplacian.

In the following we shall find it convenient to introduce the Ekman number, $E = Ta^{-1/2}$, as a measure of the importance of dissipation compared with rotation, and rescale the equations with $t \sim Et'$, $\boldsymbol{u} \sim E^{-1}\boldsymbol{u}'$. Dropping primes, and taking $\hat{\boldsymbol{z}} \cdot \nabla\times$ and $\hat{\boldsymbol{z}} \cdot \nabla \times \nabla\times$ of the momentum equation puts the governing equations into the form

$$\frac{1}{\sigma}\partial_t\nabla_\perp^2\phi - (\hat{\boldsymbol{\Omega}} \cdot \nabla)\nabla_\perp^2\psi + \frac{1}{\sigma}N_\phi(\phi,\psi) = E\nabla^2\nabla_\perp^2\phi, \tag{2.7}$$

$$\frac{1}{\sigma}\partial_t\nabla^2\nabla_\perp^2\psi + (\hat{\boldsymbol{\Omega}} \cdot \nabla)\nabla_\perp^2\phi + \frac{1}{\sigma}N_\psi(\phi,\psi) = -RaE^2\nabla_\perp^2 T + E\nabla^4\nabla_\perp^2\psi, \tag{2.8}$$

$$\partial_t T + N_T(\phi,\psi,T) = E\nabla^2 T, \tag{2.9}$$

where

$$N_\phi(\phi,\psi) = (\boldsymbol{\omega} \cdot \nabla)w - (\boldsymbol{u} \cdot \nabla)\omega_3, \tag{2.10}$$

$$N_\psi(\phi,\psi) = \hat{\boldsymbol{z}} \cdot \nabla \times \nabla \times (\boldsymbol{\omega} \times \boldsymbol{u}), \tag{2.11}$$

$$N_T(\phi,\psi,T) = \boldsymbol{u} \cdot \nabla T. \tag{2.12}$$

In the streamfunction representation these terms may be re-expressed as

$$\begin{aligned} N_\phi = &-J[\phi,\nabla_\perp^2\phi] - J[\nabla^2\psi,\nabla_\perp^2\psi] + \nabla_\perp(\nabla_\perp^2\phi)\cdot\nabla_\perp(\partial_z\psi) \\ &-\nabla_\perp(\partial_z\phi)\cdot\nabla_\perp(\nabla_\perp^2\psi) - \nabla_\perp^2\psi\nabla_\perp^2(\partial_z\phi) + \nabla_\perp^2\phi\nabla_\perp^2(\partial_z\psi), \end{aligned} \tag{2.13}$$

$$\begin{aligned} N_\psi = &-\nabla^2\left\{J[\phi,\nabla^2\psi] + J[\partial_z\phi,\partial_z\psi] - \nabla_\perp\phi\cdot\nabla_\perp(\partial_z\phi) - \nabla_\perp(\partial_z\psi)\cdot\nabla_\perp(\nabla^2\psi)\right\} \\ &-\partial_z\left\{J[\partial_z\psi,\nabla^2\phi] - J[\phi,\nabla^2\partial_z\psi] - 2J[\partial_z\phi,\nabla^2\psi] + \nabla_\perp\phi\cdot\nabla_\perp(\nabla^2\phi)\right. \\ &\left.+\nabla_\perp(\partial_z\psi)\cdot\nabla_\perp(\nabla^2\partial_z\psi) + \nabla_\perp^2\psi\nabla^2(\nabla_\perp^2\psi) + |\nabla_\perp(\partial_z\phi)|^2 + |\nabla_\perp(\nabla^2\psi)|^2 + (\nabla_\perp^2\phi)^2\right\}, \end{aligned} \tag{2.14}$$

$$N_T = -J[\phi,T] + \nabla_\perp\partial_z\psi\cdot\nabla_\perp T - \nabla_\perp^2\psi\partial_z T, \tag{2.15}$$

with the horizontal Jacobian operator $J[\cdot,\cdot] = \partial_x\cdot\,\partial_y\cdot - \partial_y\cdot\,\partial_x\cdot$. These equations are solved for a fluid confined between boundaries at fixed temperatures,

$$T(0) = 1, \qquad T(1) = 0, \tag{2.16}$$

which are impenetrable and either stress-free or no-slip:

$$\left.\begin{array}{ll} \text{stress-free:} & \psi = \partial_{zz}\psi = \partial_z\phi = 0 \\ \text{no-slip:} & \psi = \partial_z\psi = \phi = 0 \end{array}\right\} \qquad \text{at} \quad z = 0, 1. \tag{2.17}$$

As a consequence of these boundary conditions any mean flows set up in response to convection will carry no net mass flux.

2.1. *Symmetry considerations*

In rotating systems we expect, from general considerations, that spontaneous symmetry-breaking instabilities will be Hopf bifurcations producing in the nonlinear regime rotating or precessing waves (Knobloch 1994, 1996). This observation applies to systems in rotating cylinders or spheres, and is a consequence of the Coriolis force, or more abstractly of the loss of a certain reflection symmetry. For example, in an annulus heated from below and rotating about its axis the Coriolis force is responsible for the loss of reflection symmetry in vertical planes. Consequently convection with a non-zero azimuthal wavenumber sets in via a Hopf bifurcation. However, in some formulations of the problem a reflection symmetry may be inadvertently restored, and with it the possibility of steady (i.e. time-independent) convection. This is the case, for example, if the problem is formulated in a locally Cartesian geometry with identical boundary conditions on the sidewalls (Knobloch 1994, 1996). Similar considerations apply in the present problem. The nonlinear equations describing the evolution of perturbations of the conduction state $\mathbf{u} = 0$, $T = T_0(z) \equiv -\beta z$, $p(z) = p_0(z) \equiv -\frac{1}{2}\beta z^2$ take the form

$$\frac{1}{\sigma}\frac{\mathrm{D}\boldsymbol{u}}{\mathrm{D}t} + Ta^{1/2}\hat{\boldsymbol{\Omega}} \times \boldsymbol{u} = -\nabla\pi + Ra\theta\hat{\boldsymbol{z}} + \nabla^2\boldsymbol{u}, \tag{2.18}$$

$$\frac{\mathrm{D}\theta}{\mathrm{D}t} = \beta w + \nabla^2\theta, \tag{2.19}$$

$$\nabla \cdot \boldsymbol{u} = 0, \tag{2.20}$$

subject to appropriate boundary conditions in the vertical. Here $\theta \equiv T - T_0(z)$ and $\pi \equiv p - p_0(z)$. For symmetry purposes we need to distinguish between *symmetric* boundary and *non-symmetric* boundary conditions at $z = 0, 1$. By symmetric we mean that the boundary conditions on each of the four fields u, v, w, θ are the same at $z = 0, 1$, while the non-symmetric case arises when the boundary conditions on at least one of the fields differ at $z = 0, 1$. For example, the boundary conditions (2.16), (2.17) are symmetric. Suppose now that the problem is formulated in a straight channel with arbitrary orientation in the horizontal and that periodic boundary conditions are imposed along the channel direction, and consider the three reflections (cf. Knobloch 1996)

$$R_1: \quad (x, y, z) \to (-x, y, z), \quad (u, v, w, \theta, \pi) \to (-u, v, w, \theta, \pi), \tag{2.21}$$

$$R_2: \quad (x, y, z) \to (x, -y, z), \quad (u, v, w, \theta, \pi) \to (u, -v, w, \theta, \pi), \tag{2.22}$$

$$R_3: \quad (x, y, z) \to (x, y, -z), \quad (u, v, w, \theta, \pi) \to (u, v, -w, -\theta, \pi). \tag{2.23}$$

None of these reflections is by itself a symmetry of equations (2.18)–(2.20). However, the combined reflection $R \equiv R_3 \circ R_2 \circ R_1$ is a symmetry of the equations; it follows that if the sidewall boundary conditions are identical and the vertical boundary conditions symmetric then R is a symmetry of the boundary value problem. Specifically, if $(u(x, y, z), v(x, y, z), w(x, y, z), \theta(x, y, z), \pi(x, y, z))$ is a solution of the boundary value problem so is $(-u(-x, -y, -z), -v(-x, -y, -z), -w(-x, -y, -z), -\theta(-x, -y, -z), \pi(-x, -y, -z))$. However, when the boundary conditions in the vertical are non-symmetric the operation R is not a symmetry of the problem.

The presence of the symmetry R implies that the channel problem has the symmetry O(2) instead of the expected SO(2) symmetry. As mentioned above this change in symmetry is of fundamental importance both for the linear stability problem and for the nonlinear problem, and implies that the primary instability in the non-symmetric case will be a Hopf bifurcation to a rotating wave while in the symmetric case the

instability can (but need not) be a steady-state instability. This argument includes periodic boundary conditions in the sideways direction, and consequently applies to plane layers at arbitrary latitude. Note that in the special case when gravity and rotation vector are parallel the reflection R_3 is not required for the same argument to apply (Knobloch 1996). In this case symmetric boundary conditions at top and bottom are neither necessary nor sufficient for the presence of steady convection.

In the following we focus on the symmetric case. Although special for the reasons explained above this is the case that has received the most attention thus far (Hathaway *et al.* 1979, 1980). We show explicitly that, depending on the Prandtl number, both steady and oscillatory convection are possible and describe semi-analytically the properties of fully nonlinear convection of both types.

3. The linear stability problem for $E \ll 1$

In the absence of nonlinear terms equations (2.7)–(2.9) simplify to

$$\frac{1}{\sigma}\partial_t\phi - (\hat{\boldsymbol{\Omega}}\cdot\nabla)\psi = E\nabla^2\phi, \tag{3.1}$$

$$\frac{1}{\sigma}\partial_t\nabla^2\psi + (\hat{\boldsymbol{\Omega}}\cdot\nabla)\phi = -RaE^2\theta + E\nabla^4\psi, \tag{3.2}$$

$$\partial_t\theta + \nabla_\perp^2\psi = E\nabla^2\theta, \tag{3.3}$$

where $T \equiv 1 - z + \theta$. As is well known equations (3.1)–(3.3) describe the onset of both steady and oscillatory convection, with oscillatory onset preferred at low Prandtl numbers. In figure 2 we show the resulting steady eigenfunctions for $Ta = 10^{10}$ and stress-free boundary conditions; except for the presence of thin boundary layers (cf. Appendix A) the eigenfunctions for no-slip boundary conditions are essentially identical. The solid (dashed) lines show the real (imaginary) parts of the eigenfunctions. In the case of north–south oriented rolls the eigenfunctions vary on the scale of the depth of the layer, much as in the much-studied case $\vartheta = 0$ with rotation and gravity aligned.† In contrast, the eigenfunctions for east–west rolls develop rapid oscillations in the vertical, with an overall modulation on the depth scale. The small vertical scale is comparable to the horizontal scale $2\pi/k_\perp$ of the rolls. In figure 3 we show the critical Rayleigh numbers and wavenumbers for both stress-free and no-slip boundary conditions and for both roll orientations. In addition to revealing unexpected nonmonotonic behaviour for moderate rotation rates the figure confirms that for sufficiently large rotation rates $Ra \sim Ta^{2/3}$ and $k_\perp \sim Ta^{1/6}$, as noted by Hathaway *et al.* (1980). This asymptotic regime is reached by $Ta = 10^8$ for stress-free boundary conditions, but is delayed to $Ta > 10^{10}$ for no-slip boundary conditions; in the former case the asymptotic Rayleigh number is approached from above, while in the latter it is approached from below, with the asymptotic wavenumber approached from below in both cases. These results motivate the scaling

$$\partial_x, \partial_y = E^{-1/3}(\partial_{x'}, \partial_{y'}), \qquad \partial_z = E^{-1/3}(\partial_{z'} + E^{1/3}\mathrm{D}), \qquad Ra = E^{-4/3}Ra', \tag{3.4}$$

with $\mathrm{D} \equiv \partial_Z$. For oscillatory convection we let, in addition, $\partial_t = E^{1/3}\partial_{t'}$. Note that the same scaling is used for stress-free and no-slip boundary conditions (cf. Clune & Knobloch 1993). Indeed, as we shall see, the stress-free and no-slip results become

† These cases are in fact related by the transformation $Ta^{1/2} \to Ta^{1/2}\cos\vartheta$ (Chandrasekhar 1961).

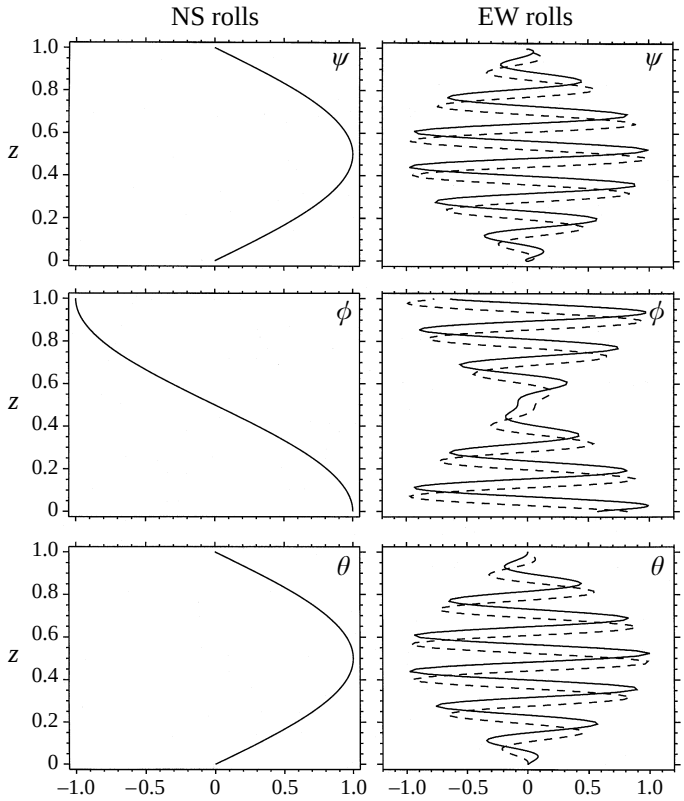

FIGURE 2. Profiles of steady critical north–south (NS) and east–west (EW) eigenfunctions ψ, ϕ and θ computed from equations (3.1)–(3.3) with stress-free boundary conditions and $Ta = 10^{10}$. The solid (dashed) lines indicate the real (imaginary) parts. Note the rapid oscillations in the profile of the east–west eigenfunctions forced by the Taylor–Proudman constraint.

essentially indistinguishable in the large rotation limit as the boundary layers at the top and bottom required in the two cases become thinner and thinner.

The scaling (3.4) forms the basis for the asymptotic solution of both the linear and nonlinear problems described below. In the remainder of this section we demonstrate its usefulness by solving the eigenvalue problem

$$-(\hat{\boldsymbol{\Omega}}\cdot\nabla)^2\psi = E^2(\nabla^6\psi - Ra\nabla_\perp^2\psi) \tag{3.5}$$

for the onset of steady convection, and comparing the result with the exact solution. With the scaling (3.4) the eigenvalue problem becomes (dropping primes)

$$-(\hat{\boldsymbol{\Omega}}\cdot\nabla_0)^2\psi = E^{1/3}(2\hat{\Omega}_3(\hat{\boldsymbol{\Omega}}\cdot\nabla_0)\mathrm{D})\psi + E^{2/3}(\hat{\Omega}_3^2\mathrm{D}^2 + \nabla_0^6 - Ra\nabla_{0\perp}^2)\psi + O(E), \tag{3.6}$$

where

$$\nabla = \nabla_0 + E^{1/3}\mathrm{D}, \quad \nabla_0 = (\partial_x, \partial_y, \partial_z), \quad \nabla_{0\perp} = (\partial_x, \partial_y, 0), \tag{3.7}$$

$$\nabla^2 = (\nabla_0^2 + 2E^{1/3}\partial_z\mathrm{D} + E^{2/3}\mathrm{D}^2), \quad \nabla_0^2 = \partial_{xx} + \partial_{yy} + \partial_{zz}. \tag{3.8}$$

This equation may be solved analytically by posing the following expansion for ψ,

$$\psi = \psi_0 + E^{1/3}\psi_{1/3} + E^{2/3}\psi_{2/3} + \cdots. \tag{3.9}$$

This *Ansatz* leads to a sequence of linear inhomogeneous problems, the first of which

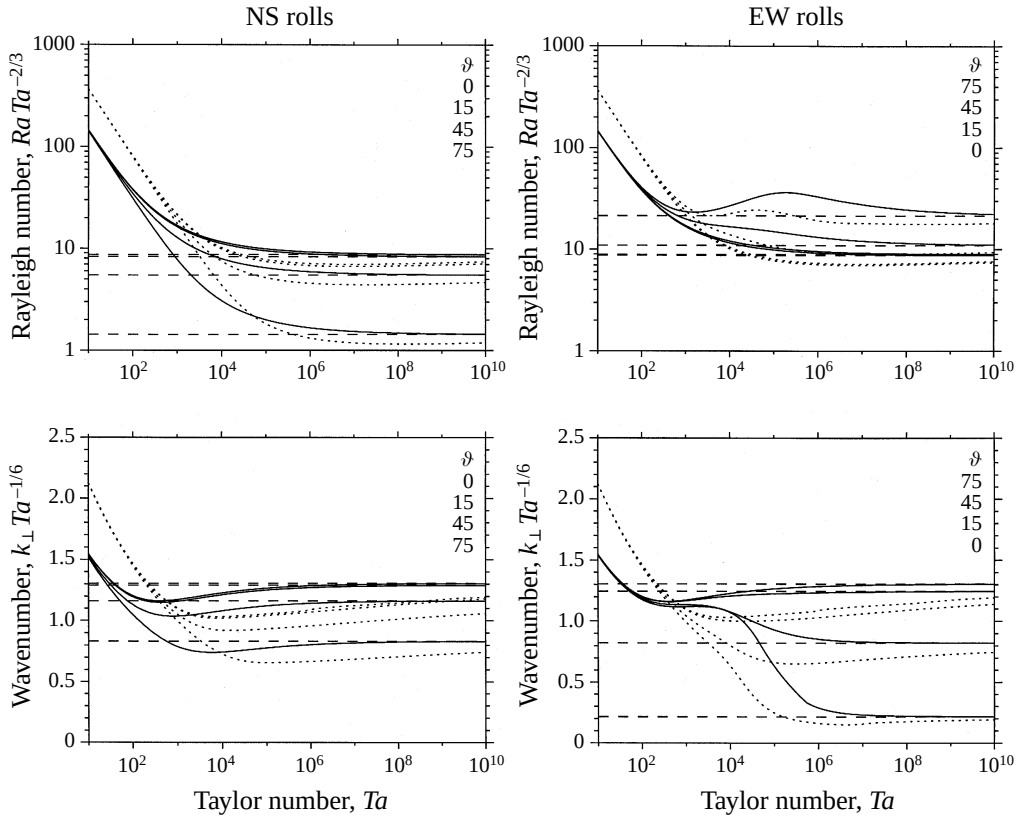

FIGURE 3. Normalized critical Rayleigh numbers and wavenumbers at various colatitudes ϑ for steady NS and EW rolls as functions of the Taylor number computed from equations (3.1)–(3.3) with stress-free (solid lines) and no-slip (dotted lines) boundary conditions. The dashed lines indicate the corresponding asymptotic predictions $Ra_{\rm crit}$, $k_{0\perp{\rm crit}}$.

is

$$-(\hat{\boldsymbol{\Omega}}\cdot\nabla_0)^2\psi_0 = 0. \tag{3.10}$$

The solution to this equation can be written in the form of a normal mode,

$$\psi_0 = \psi_S(Z)\exp(\mathrm{i}\boldsymbol{k}_0\cdot\boldsymbol{x}) + \text{c.c.} \quad \text{with} \quad \boldsymbol{k}_0\cdot\hat{\boldsymbol{\Omega}} \equiv 0, \tag{3.11}$$

and represents the solution in the bulk of the fluid layer; it is none other than the Taylor–Proudman solution which requires the normal mode motions of the fluid to be perpendicular to the rotation axis. In terms of the wavevector $\boldsymbol{k}_0 = (k_{0x}, k_{0y}, k_{0z})$ the Taylor–Proudman constraint can be rewritten as $k_{0z} = -k_{0y}\tan\vartheta$.

At $O(E^{1/3})$,

$$-(\hat{\boldsymbol{\Omega}}\cdot\nabla_0)^2\psi_{1/3} = [2\hat{\Omega}_3(\hat{\boldsymbol{\Omega}}\cdot\nabla_0)\mathrm{D}]\psi_0. \tag{3.12}$$

The right-hand side of this equation is identically zero since $\boldsymbol{k}_0\cdot\hat{\Omega} \equiv 0$. Hence without loss of generality we set $\psi_{1/3} \equiv 0$.

At $O(E^{2/3})$,

$$-(\hat{\boldsymbol{\Omega}}\cdot\nabla_0)^2\psi_{2/3} = [\hat{\Omega}_3^2\mathrm{D}^2 - (k_0^6 - Rak_{0\perp}^2)]\psi_0, \tag{3.13}$$

with $k_0 = |\boldsymbol{k}_0|$ and $k_{0\perp}^2 = k_{0x}^2 + k_{0y}^2$. All terms on the right-hand side at this order are resonant with respect to the zeroth-order operator. The solvability condition is

therefore

$$[\hat{\Omega}_3^2 \mathrm{D}^2 - (k_0^6 - Rak_{0\perp}^2)]\psi_S = 0, \qquad \psi_S(0) = \psi_S(1) = 0. \tag{3.14}$$

This equation is of second order in Z; consequently the only boundary conditions that may be applied are those enforcing impenetrability. The above equation is therefore an outer (or bulk) solution for the fluid layer. It represents the large-scale modulation of the Taylor column due to the finite depth of the convecting layer, and implies the existence of boundary layers near $Z = 0, 1$ the solution to which satisfy the correct velocity boundary conditions (see Appendix A). These solutions must be matched to the bulk solution.

At the onset of convection the outer solution is given by

$$\psi_0 = \left[A \exp(\mathrm{i}\boldsymbol{k}_0 \cdot \boldsymbol{x}) + \text{c.c.}\right] \sin(n\pi Z), \qquad Ra = \frac{k_0^6 + n^2\pi^2 \cos^2 \vartheta}{k_{0\perp}^2}, \tag{3.15}$$

where A is a constant amplitude. We focus on the fundamental mode $n = 1$ which is the most unstable mode. Recalling that $k_{0z} = -k_{0y} \tan \vartheta$ and setting $(k_{0x}, k_{0y}) = k_{0\perp}(\cos \chi, \sin \chi)$ gives

$$Ra_0 = k_{0\perp}^4 (1 + \sin^2 \chi \tan^2 \vartheta)^3 + \frac{\pi^2 \cos^2 \vartheta}{k_{0\perp}^2}. \tag{3.16}$$

The minimum critical Rayleigh number and the corresponding wavenumber are thus

$$Ra_{\text{crit}} = \tfrac{3}{2}(2\pi^4 \cos^4 \vartheta)^{1/3}(1 + \sin^2 \chi \tan^2 \vartheta), \quad k_{0\perp\text{crit}} = \left[\frac{\pi^2 \cos^2 \vartheta}{2(1 + \sin^2 \chi \tan^2 \vartheta)^3}\right]^{1/6}. \tag{3.17}$$

The corresponding results for the critical Rayleigh number and frequency at onset of oscillatory convection are

$$Ra_0 = 2(1 + \sigma)\left[k_{0\perp}^4 (1 + \sin^2 \chi \tan^2 \vartheta)^3 + \left(\frac{\sigma}{1 + \sigma}\right)^2 \frac{\pi^2 \cos^2 \vartheta}{k_{0\perp}^2}\right], \tag{3.18}$$

$$\omega_0^2 = \sigma^2 \left[\left(\frac{1 - \sigma}{1 + \sigma}\right) \frac{\pi^2 \cos^2 \vartheta}{k_{0\perp}^2 (1 + \sin^2 \chi \tan^2 \vartheta)} - k_{0\perp}^4 (1 + \sin^2 \chi \tan^2 \vartheta)^2\right]. \tag{3.19}$$

The minimum critical Rayleigh number and the corresponding wavenumber and frequency thus are

$$Ra_{\text{crit}} = 3(1 + \sigma)\left(\frac{\sigma}{1 + \sigma}\right)^{4/3} (2\pi^4 \cos^4 \vartheta)^{1/3}(1 + \sin^2 \chi \tan^2 \vartheta), \tag{3.20}$$

$$k_{0\perp\text{crit}} = \left(\frac{\sigma}{1 + \sigma}\right)^{1/3} \left[\frac{\pi^2 \cos^2 \vartheta}{2(1 + \sin^2 \chi \tan^2 \vartheta)^3}\right]^{1/6}, \tag{3.21}$$

$$\omega_{\text{crit}}^2 = \left(\frac{\sigma}{1 + \sigma}\right)^{4/3} \left(\frac{\pi^2 \cos^2 \vartheta}{2}\right)^{2/3} (2 - 3\sigma^2). \tag{3.22}$$

Comparison with the corresponding steady-state result shows that the first bifurcation is a Hopf one if $\sigma < \sigma^* \approx 0.676\,605$, as derived by Chandrasekhar (1961).

Figure 4 illustrates the marginal stability curves (3.16), (3.18) for the onset of steady and oscillatory convection in the scaled Rayleigh number–wavenumber space when $\sigma = 0.4547$. Results for both north–south rolls ($\chi = 0$) and east–west rolls ($\chi = \frac{1}{2}\pi$) are shown. As indicated in figure 4(*b*) the wavenumber $k_{0\perp} = k_{0TB}$, defined by $\omega_0 = 0$,

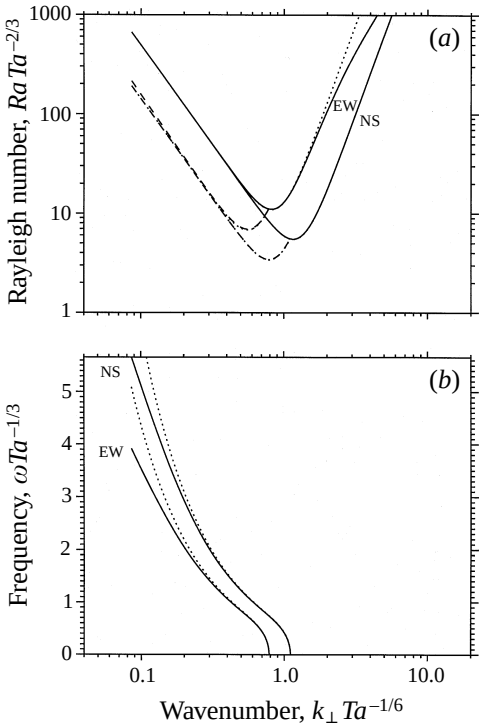

FIGURE 4. (*a*) The normalized and asymptotic neutral stability curves for NS and EW rolls when $\sigma = 0.4547$. The solid (broken) lines indicate steady (oscillatory) onset for stress-free boundaries; the dotted lines indicate the asymptotic relations (3.16), (3.18). (*b*) The normalized critical (solid lines) and asymptotic (dotted lines) frequencies (3.19) at onset.

provides an upper limit on the wavenumbers for which oscillations are present. The asymptotic predictions (3.17) for $Ra_{\rm crit}$ are indicated by dashed lines in figure 3 and are evidently in excellent agreement with the exact results. This agreement extends to the eigenfunction itself. In figure 5 we show the real (solid line) and imaginary (dashed line) parts of the streamfunction $\psi_S(Z)\exp {\rm i}k_{0z}z$ for steady north–south (hereafter NS) and east–west (hereafter EW) rolls at $\vartheta = 45^\circ$ obtained from the asymptotic analysis, and compare them with the exact results for stress-free boundary conditions and $Ta = 10^{10}$ (dashed-dotted and dotted lines, respectively). For NS rolls $k_{0z} = 0$ and $\psi(Z,z)$ is real; the agreement between the exact and asymptotic results is essentially perfect. For EW rolls the two sets of curves remain indistinguishable in the bulk but departures from the asymptotic results are evident in the Ekman boundary layers at the top and bottom. The thickness of these is $O(E^{1/2}) \approx 0.3\%$ (see Appendix A), a result that is consistent with the exact results. Note that such boundary layers are present even in the stress-free case, provided $0 < \vartheta < \pi/2$, $\chi \neq 0$, i.e. they are absent only for NS rolls (cf. figure 5). The results (3.15)–(3.22) thus represent accurate analytic approximations to the exact results for both sets of boundary conditions in the limit of rapid rotation, generalizing existing results to a tilted f-plane.

Observe that the chosen scaling (3.4) supposes that $k_z \sim O(1)$ implying $\vartheta \ll \pi/2$ for the above derivation to remain asymptotic. In contrast the Taylor–Proudman constraint in the limit $\vartheta \to 0$ implies $k_z \to 0$. In this limit both the Rayleigh number and the wavenumber converge to the large-rotation scaling of Chandrasekhar (1961)

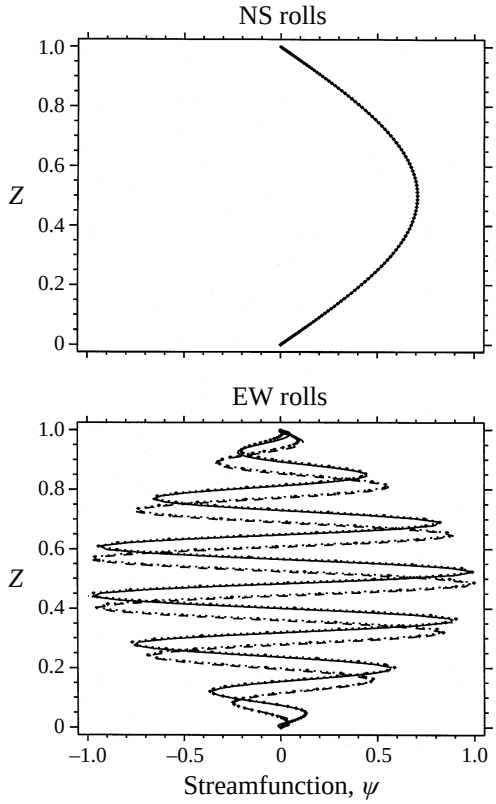

FIGURE 5. Comparison of the asymptotic and exact eigenfunctions ψ for steady NS and EW rolls at latitude 45° for $Ta = 10^{10}$ and stress-free boundary conditions. The solid (dashed) lines show the real (imaginary) parts of the asymptotic result while the dashed-dotted (dotted) lines show the corresponding exact results. Differences can be discerned only for EW rolls and then only in the boundary layers at top and bottom.

and Bassom & Zhang (1994) (see figure 3). Although there exists no separation of vertical scales in this limit the expansion procedure remains valid.

The critical Rayleigh numbers (3.17), (3.20) are least when $\chi = 0$ (see figures 3, 4). It follows that rolls oriented in the north–south direction are the first to set in as the Rayleigh number increases, followed by other orientations with increasing *Ra*. In particular east–west rolls ($\chi = \frac{1}{2}\pi$) are the last to come in (cf. Hathaway & Somerville 1983). These two types of roll solutions have substantially different properties. In particular NS rolls are characterized by $k_{0y} = k_{0z} = 0$, while EW rolls have $k_{0x} = 0$, but $k_{0y} \neq 0$, $k_{0z} \neq 0$. Thus the former have no small-scale structure in the vertical, while the latter do. We are therefore led to consider the following scenario: at onset NS rolls set in, but with increasing *Ra* other orientations come in and with them the small-scale structure in the vertical imposed by the Taylor–Proudman constraint. The existence of this small scale in the vertical has dramatic consequences for the transport properties of the resulting nonlinear convection. In subsequent sections we contrast the horizontal heat fluxes produced by these two types of nonlinear states, and the mean flows they generate.

4. The nonlinear problem for $E \ll 1$: steady convection

We now extend the two-scale asymptotic analysis employed in the preceding section into the nonlinear regime, starting with steady convection. We write $T = \overline{T}(Z) + \theta(x, y, z; Z)$, where

$$\overline{T} \equiv \int T \mathrm{d}x\mathrm{d}y\mathrm{d}z \tag{4.1}$$

denotes an average over small scales and $\theta(x, y, z; Z)$ is the fluctuating part of the temperature. In terms of the scaled variables

$$\phi = E\phi', \qquad \psi = E^{4/3}\psi', \qquad \theta = E^{1/3}\theta' \tag{4.2}$$

equations (2.7)–(2.9) become, after dropping primes,

$$-(\hat{\boldsymbol{\Omega}} \cdot \nabla)\nabla_{0\perp}^2 \psi = E^{1/3}\left(\nabla^2 \nabla_{0\perp}^2 \phi - \frac{1}{\sigma} N_\phi(\phi, \psi)\right) + O(E^{2/3}), \tag{4.3}$$

$$(\hat{\boldsymbol{\Omega}} \cdot \nabla)\nabla_{0\perp}^2 \phi = E^{1/3}\left(\nabla^4 \nabla_{0\perp}^2 \psi - Ra\nabla_{0\perp}^2 \theta - \frac{1}{\sigma} N_\psi(\phi, \psi)\right) + O(E^{2/3}), \tag{4.4}$$

$$-\nabla_{0\perp}^2 \psi \mathrm{D}\overline{T} + (N_T(\phi, \psi, \theta) - \overline{N_T(\phi, \psi, \theta)}) = \nabla^2 \theta + O(E^{1/3}), \tag{4.5}$$

$$\overline{\nabla_{0\perp}\mathrm{D}\psi \cdot \nabla_{0\perp}\theta - \nabla_{0\perp}^2 \psi \mathrm{D}\theta} = \mathrm{D}^2 \overline{T} + O(E^{1/3}). \tag{4.6}$$

To obtain these equations we have used the fact that at leading order

$$\overline{N_T(\phi, \psi, \theta)} \equiv 0. \tag{4.7}$$

In the following we consider two-dimensional solutions only, i.e. rolls. For this planform $N_\phi(\phi, \psi), N_\psi(\phi, \psi), N_T(\phi, \psi, \theta) \equiv 0$ to leading order, and hence

$$-(\hat{\boldsymbol{\Omega}} \cdot \nabla_0)\nabla_{0\perp}^2 \psi = E^{1/3}(\hat{\Omega}_3 \mathrm{D}\nabla_{0\perp}^2 \phi + \nabla_0^2 \nabla_{0\perp}^2 \phi) + O(E^{2/3}), \tag{4.8}$$

$$(\hat{\boldsymbol{\Omega}} \cdot \nabla_0)\nabla_{0\perp}^2 \phi = E^{1/3}(-\hat{\Omega}_3 \mathrm{D}\nabla_{0\perp}^2 \phi + \nabla_0^4 \nabla_{0\perp}^2 \psi - Ra\nabla_{0\perp}^2 \theta) + O(E^{2/3}), \tag{4.9}$$

$$-\nabla_{0\perp}^2 \psi \mathrm{D}\overline{T} = \nabla_0^2 \theta + O(E^{1/3}), \tag{4.10}$$

$$\overline{\nabla_{0\perp}\mathrm{D}\psi \cdot \nabla_{0\perp}\theta - \nabla_{0\perp}^2 \psi \mathrm{D}\theta} = \mathrm{D}^2 \overline{T} + O(E^{1/3}). \tag{4.11}$$

These equations are solved by an asymptotic expansion of the form

$$\begin{pmatrix} \boldsymbol{\Psi} \\ \overline{T} \end{pmatrix} = \begin{pmatrix} \boldsymbol{\Psi}_0 \\ \overline{T}_0 \end{pmatrix} + E^{1/3}\begin{pmatrix} \boldsymbol{\Psi}_{1/3} \\ \overline{T}_{1/3} \end{pmatrix} + E^{2/3}\begin{pmatrix} \boldsymbol{\Psi}_{2/3} \\ \overline{T}_{2/3} \end{pmatrix} + \cdots, \tag{4.12}$$

where $\boldsymbol{\Psi} \equiv (\phi, \psi, \theta)^T$. At $O(E^0)$ one obtains

$$-(\hat{\boldsymbol{\Omega}} \cdot \nabla_0)\nabla_{0\perp}^2 \psi_0 = 0, \qquad (\hat{\boldsymbol{\Omega}} \cdot \nabla_0)\nabla_{0\perp}^2 \phi_0 = 0, \tag{4.13}$$

$$-\nabla_{0\perp}^2 \psi_0 \mathrm{D}\overline{T}_0 = \nabla_0^2 \theta_0, \qquad \overline{\nabla_{0\perp}\mathrm{D}\psi_0 \cdot \nabla_{0\perp}\theta_0 - \nabla_{0\perp}^2 \psi_0 \mathrm{D}\theta_0} = \mathrm{D}^2 \overline{T}_0. \tag{4.14}$$

The bulk convective solution to these equations may be described in terms of a steady normal mode satisfying the Taylor–Proudman constraint:

$$\begin{pmatrix} \phi_0 \\ \psi_0 \\ \theta_0 \end{pmatrix} = \begin{pmatrix} \phi_S(Z) \\ \psi_S(Z) \\ \theta_S(Z) \end{pmatrix} \exp(\mathrm{i}\boldsymbol{k}_0 \cdot \boldsymbol{x}) + \text{c.c.} \tag{4.15}$$

with $\boldsymbol{k}_0 \cdot \hat{\boldsymbol{\Omega}} \equiv 0$ and

$$k_0^2 \theta_S = -k_{0\perp}^2 \mathrm{D}\overline{T}_0 \psi_S. \tag{4.16}$$

At $O(E^{1/3})$

$$-(\hat{\boldsymbol{\Omega}}\cdot\nabla_0)\nabla_{0\perp}^2\psi_{1/3} = (\hat{\Omega}_3\mathrm{D}\nabla_{0\perp}^2\psi_0 + \nabla_0^2\nabla_{0\perp}^2\phi_0), \tag{4.17}$$

$$(\hat{\boldsymbol{\Omega}}\cdot\nabla_0)\nabla_{0\perp}^2\phi_{1/3} = (-\hat{\Omega}_3\mathrm{D}\nabla_{0\perp}^2\phi_0 + \nabla_0^4\nabla_{0\perp}^2\psi_0 - Ra\nabla_{0\perp}^2\theta_0). \tag{4.18}$$

Applying the solvability condition gives the governing equations for the bulk,

$$\hat{\Omega}_3\mathrm{D}\psi_S = k_0^2\phi_S, \tag{4.19}$$

$$-\hat{\Omega}_3\mathrm{D}\phi_S + k_0^4\psi_S - Ra\theta_S = 0, \tag{4.20}$$

together with

$$k_{0\perp}^2\mathrm{D}(\psi_S\theta_S^* + \text{c.c.}) = \mathrm{D}^2\overline{T}_0. \tag{4.21}$$

Thus

$$\hat{\Omega}_3^2\mathrm{D}^2\psi_S - (k_0^6 + k_{0\perp}^2 Ra\mathrm{D}\overline{T}_0)\psi_S = 0, \tag{4.22}$$

$$-2\frac{k_{0\perp}^4}{k_0^2}\mathrm{D}(|\psi_S|^2\mathrm{D}\overline{T}_0) = \mathrm{D}^2\overline{T}_0. \tag{4.23}$$

The latter equation can be solved for the mean temperature gradient,

$$\mathrm{D}\overline{T}_0 = -\frac{Kk_0^2}{k_0^2 + 2k_{0\perp}^4|\psi_S|^2}, \tag{4.24}$$

where K is a constant determined by the temperature boundary conditions $\overline{T}_0 = 1$ at $Z = 0$ and $\overline{T}_0 = 0$ at $Z = 1$:

$$K = \left[\int_0^1 \frac{k_0^2}{k_0^2 + 2k_{0\perp}^4|\psi_S|^2}\mathrm{d}Z\right]^{-1}. \tag{4.25}$$

In fact, as shown in §6, K represents at leading order the *Nusselt number* averaged over small scales. Thus the outer solution for steady nonlinear convection is described by the single equation

$$\hat{\Omega}_3^2\mathrm{D}^2\psi_S + k_0^2\left(\frac{k_{0\perp}^2 RaK}{k_0^2 + 2k_{0\perp}^4|\psi_S|^2} - k_0^4\right)\psi_S = 0, \qquad \psi_S(0) = \psi_S(1) = 0. \tag{4.26}$$

This equation represents a nonlinear eigenvalue problem which we solve on a discretized one-dimensional mesh using an iterative Newton–Raphson–Kantorovich (NRK) scheme (Henrici 1962; Cash & Singhal 1982) with $O(10^{-10})$ accuracy in the L_2 norm of $\psi_S(Z)$ and the corresponding eigenvalue K. The scaled Rayleigh number Ra is used as the control parameter. Note that when $\hat{\Omega}_3^2(=\cos^2\vartheta) = 1$ equation (4.26) reduces to that derived by Bassom & Zhang (1994); our f-plane generalization ($\vartheta \neq 0$) required the introduction of a small scale in the vertical, and hence a multiple-scale analysis, as described above. However, the solution at general latitude continues to be supercritical and independent of the Prandtl number.

In figure 6 we show the resulting streamlines at latitude 45° for (*a*) NS rolls, and (*b*) EW rolls, both for $Ra = 100$. As already mentioned the NS roll boundaries remain vertical, while the EW rolls become inclined towards the north as a result of the Taylor–Proudman constraint. Both solutions are constructed using the critical horizontal wavenumber $k_{0\perp\mathrm{crit}}$ given in equation (3.17). However, for purposes of illustration we have treated the two vertical scales z, Z as identical; it should be borne in mind that not only are the rolls very narrow in the horizontal, but the EW ones also have a comparably small scale superposed in the vertical, as suggested by

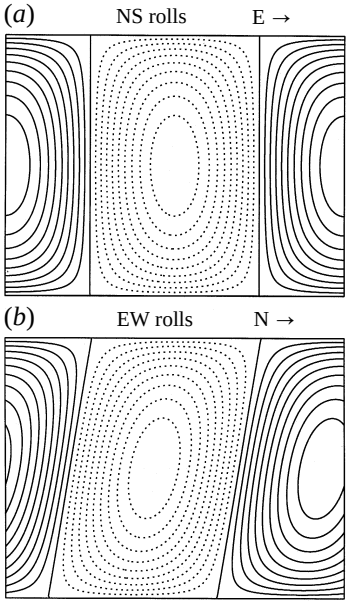

FIGURE 6. Streamlines $\psi = \text{const.}$ at 45° latitude and $Ra\,E^{4/3} = 100$ for (a) NS rolls, and (b) EW rolls. In (b) latitude increases to the right (northern hemisphere). Note the poleward tilt of the rolls in figure (b); the figure is drawn for the case in which the slow and fast scales in the vertical are indistinguishable (see text). Solid (dotted) lines indicate clockwise (counterclockwise) motion.

figure 5. As the rotation rate increases the Taylor–Proudman constraint is obeyed better and better, and the roll inclination (with respect to the local vertical) of the EW rolls comes closer and closer to being the colatitude ϑ. The amplitude of these fully nonlinear solutions can be discerned from figure 7 which shows the vertical profiles of the mean temperature $\overline{T}_0(Z)$ and the streamfunction $\psi_S(Z)$ at 45° latitude for both orientations and several values of the Rayleigh number. By $Ra = 100$, the case illustrated in figure 6, the profiles are already highly nonlinear, certainly well beyond the regimes accessible via weakly nonlinear theory. The corresponding Nusselt number K is shown as a function of the applied Rayleigh number in figure 8, with the solid (dashed) lines showing the results for NS (EW) rolls, respectively. Observe that while there is a large difference between the Nusselt numbers at latitude 15° ($\vartheta = 75°$) this difference gradually diminishes as ϑ decreases; of course when $\vartheta = 0$ the resulting orientational degeneracy implies that all orientations of the rolls carry the same heat flux.

As already indicated the solution obtained above represents the solution in the bulk of the fluid. The complete solution requires the presence of thin boundary layers through which the bulk solution is matched to the imposed boundary conditions. In Appendix A we summarize the results of this procedure. In particular we conclude that the required boundary layers are passive and hence have no effect asymptotically either on the leading-order bulk solution or on the corresponding eigenvalue K.

5. The nonlinear problem for $E \ll 1$: overstable convection

The symmetry properties of the basic equations discussed in §2.1 imply that the purely imaginary eigenvalues at a Hopf bifurcation will have multiplicity two. Standard weakly nonlinear analysis (eg. Knobloch & Silber 1990) shows that in this

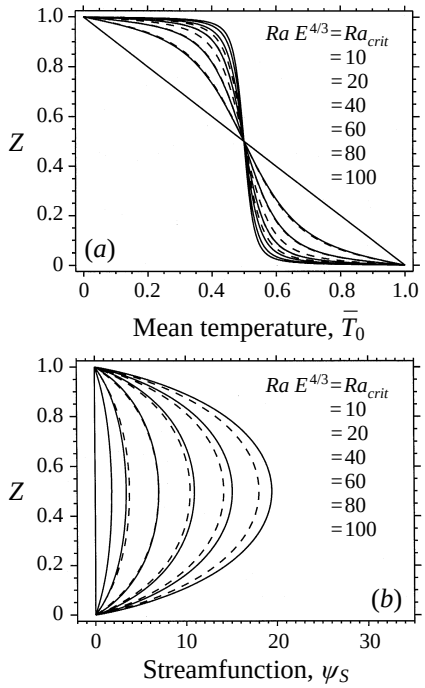

FIGURE 7. (*a*) The mean temperature profile $\overline{T}_0(Z)$ and (*b*) streamfunction profile $\psi_S(Z)$ at latitude 45° for NS oriented rolls (solid lines) and EW oriented rolls (dashed lines) at different values of the (scaled) Rayleigh number $Ra\,E^{4/3}$.

case two solution branches bifurcate from the trivial (conduction) state: a branch of travelling waves (hereafter TW) and a branch of standing waves (hereafter SW). In the asymptotic analysis of the overstable case we shall find that the leading-order nonlinearity arises from the deformation of the mean temperature gradient, much as in the steady case discussed in the previous section. As a result we shall find a degeneracy between the TW and SW: both solutions can be constructed from the solution of the *same* nonlinear eigenvalue problem. Consequently both have the same (time-averaged) Nusselt number and nonlinear oscillation frequency. In particular the competition between these two solutions requires the use of the slow timescale $O(E^{-1/3})$ (cf. Julien & Knobloch 1997) and the computation of subdominant terms. Nonetheless, in what follows we construct solutions of both types and study their transport properties since these are determined by the leading-order solution.

With $\partial_t = E^{1/3}\partial_{t'}$, the equations describing two-dimensional overstable convection take the form, cf. (4.8)–(4.11),

$$-(\hat{\boldsymbol{\Omega}}\cdot\nabla_0)\nabla_{0\perp}^2\psi = E^{1/3}\left(\hat{\Omega}_3\mathrm{D}\nabla_{0\perp}^2\psi + \nabla_0^2\nabla_{0\perp}^2\phi - \frac{1}{\sigma}\partial_t\nabla_{0\perp}^2\psi\right) + O(E^{2/3}), \tag{5.1}$$

$$(\hat{\boldsymbol{\Omega}}\cdot\nabla_0)\nabla_{0\perp}^2\phi = E^{1/3}\left(-\hat{\Omega}_3\mathrm{D}\nabla_{0\perp}^2\phi + \nabla_0^4\nabla_{0\perp}^2\psi - \frac{1}{\sigma}\partial_t\nabla_0^2\nabla_{0\perp}^2\psi - Ra\nabla_{0\perp}^2\theta\right) + O(E^{2/3}), \tag{5.2}$$

$$\partial_t\theta - \nabla_{0\perp}^2\psi\mathrm{D}\overline{T} = \nabla_0^2\theta + O(E^{1/3}), \tag{5.3}$$

$$\overline{\nabla_{0\perp}\mathrm{D}\psi\cdot\nabla_{0\perp}\theta - \nabla_{0\perp}^2\psi\mathrm{D}\theta} = \mathrm{D}^2\overline{T} + O(E^{1/3}). \tag{5.4}$$

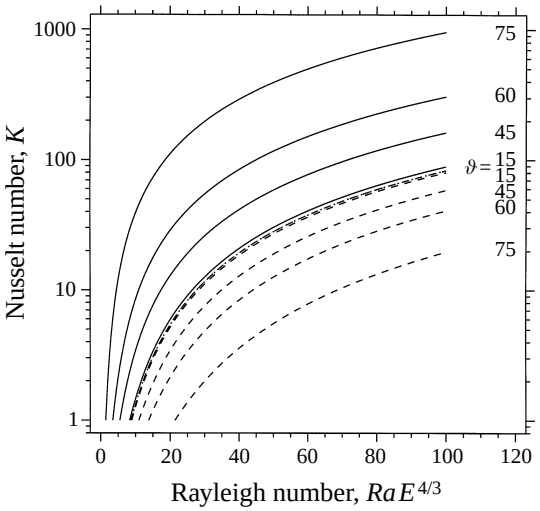

FIGURE 8. The Nusselt number K as a function of the (scaled) Rayleigh number $Ra\,E^{4/3}$ for several different colatitudes ϑ. Solid (dashed) lines indicate results for NS (EW) oriented rolls.

In writing these equations we have extended the meaning of the overbar to include a time average as well. Proceeding as in §4, we find that equations (4.13), (4.14*b*) are unchanged, while (4.14*a*) is replaced by

$$-\nabla_{0\perp}^2\psi_0 \mathrm{D}\overline{T}_0 = (\nabla_0^2 - \partial_t)\theta_0. \tag{5.5}$$

The bulk convective solution to these equations may be described in terms of a superposition of left- and right-travelling waves,

$$\begin{pmatrix}\phi_0\\ \psi_0\\ \theta_0\end{pmatrix} = \begin{pmatrix}\phi_L(Z)\\ \psi_L(Z)\\ \theta_L(Z)\end{pmatrix}\exp(\mathrm{i}\omega t + \mathrm{i}\boldsymbol{k}_0\cdot\boldsymbol{x}) + \begin{pmatrix}\phi_R(Z)\\ \psi_R(Z)\\ \theta_R(Z)\end{pmatrix}\exp(\mathrm{i}\omega t - \mathrm{i}\boldsymbol{k}_0\cdot\boldsymbol{x}) + \text{c.c.}, \tag{5.6}$$

satisfying the Taylor–Proudman constraint $\boldsymbol{k}_0\cdot\hat{\boldsymbol{\Omega}} \equiv 0$, and

$$(k_0^2 + \mathrm{i}\omega)\theta_L = -k_{0\perp}^2 \mathrm{D}\overline{T}_0\psi_L, \qquad (k_0^2 + \mathrm{i}\omega)\theta_R = -k_{0\perp}^2 \mathrm{D}\overline{T}_0\psi_R. \tag{5.7}$$

At $O(E^{1/3})$

$$-(\hat{\boldsymbol{\Omega}}\cdot\nabla_0)\nabla_{0\perp}^2\psi_{1/3} = E^{1/3}\left(\hat{\Omega}_3\mathrm{D}\nabla_{0\perp}^2\psi_0 + \nabla_0^2\nabla_{0\perp}^2\phi_0 - \frac{1}{\sigma}\partial_t\nabla_{0\perp}^2\phi_0\right), \tag{5.8}$$

$$(\hat{\boldsymbol{\Omega}}\cdot\nabla_0)\nabla_{0\perp}^2\phi_{1/3} = E^{1/3}\left(-\hat{\Omega}_3\mathrm{D}\nabla_{0\perp}^2\phi_0 + \nabla_0^4\nabla_{0\perp}^2\psi_0 - \frac{1}{\sigma}\partial_t\nabla_0^2\nabla_{0\perp}^2\psi_0 - Ra\nabla_{0\perp}^2\theta_0\right). \tag{5.9}$$

The solvability condition gives the governing equations for the bulk,

$$\hat{\Omega}_3\mathrm{D}\psi_L - (k_0^2 + \mathrm{i}\omega/\sigma)\phi_L = 0, \qquad \hat{\Omega}_3\mathrm{D}\psi_R - (k_0^2 + \mathrm{i}\omega/\sigma)\phi_R = 0, \tag{5.10}$$

$$-\hat{\Omega}_3\mathrm{D}\phi_L - Ra\theta_L + (k_0^2 + \mathrm{i}\omega/\sigma)k_0^2\psi_L = 0, \qquad -\hat{\Omega}_3\mathrm{D}\phi_R - Ra\theta_R + (k_0^2 + \mathrm{i}\omega/\sigma)k_0^2\psi_R = 0, \tag{5.11}$$

together with

$$k_{0\perp}^2\mathrm{D}(\psi_L\theta_L^* + \psi_R\theta_R^* + \psi_L^*\theta_L + \psi_R^*\theta_R) = \mathrm{D}^2\overline{T}_0. \tag{5.12}$$

Eliminating $\phi_L, \theta_L, \phi_R, \theta_R$ leads to the reduced equations

$$-\hat{\Omega}_3^2 \mathrm{D}^2\psi_L + \frac{\left(k_0^2 + \mathrm{i}\omega/\sigma\right)}{\left(k_0^2 + \mathrm{i}\omega\right)} k_{0\perp}^2 Ra \mathrm{D}\overline{T}_0 \psi_L + k_0^2 \left(k_0^2 + \mathrm{i}\omega/\sigma\right)^2 \psi_L = 0, \tag{5.13}$$

$$-\hat{\Omega}_3^2 \mathrm{D}^2\psi_R + \frac{\left(k_0^2 + \mathrm{i}\omega/\sigma\right)}{\left(k_0^2 + \mathrm{i}\omega\right)} k_{0\perp}^2 Ra \mathrm{D}\overline{T}_0 \psi_R + k_0^2 \left(k_0^2 + \mathrm{i}\omega/\sigma\right)^2 \psi_R = 0, \tag{5.14}$$

$$-\frac{2k_0^2 k_{0\perp}^4}{(k_0^4 + \omega^2)} \mathrm{D}[(|\psi_L|^2 + |\psi_R|^2)\mathrm{D}\overline{T}_0] = \mathrm{D}^2\overline{T}_0. \tag{5.15}$$

The latter equation can be solved for the mean temperature gradient,

$$\mathrm{D}\overline{T}_0 = -K \frac{k_0^4 + \omega^2}{k_0^4 + \omega^2 + 2k_0^2 k_{0\perp}^4 (|\psi_L|^2 + |\psi_R|^2)}. \tag{5.16}$$

To satisfy the temperature boundary conditions, $\overline{T}_0 = 1$ at $Z = 0$, and $\overline{T}_0 = 0$ at $Z = 1$,

$$K = \left[\int_0^1 \frac{k_0^4 + \omega^2}{k_0^4 + \omega^2 + 2k_0^2 k_{0\perp}^4 (|\psi_L|^2 + |\psi_R|^2)} \mathrm{d}Z \right]^{-1}. \tag{5.17}$$

Physically, K is the Nusselt number averaged over both time and small scales. Eliminating $\mathrm{D}\overline{T}_0$ then gives

$$-\hat{\Omega}_3^2 \mathrm{D}^2\psi_L - \frac{k_{0\perp}^2 \left(k_0^2 + \mathrm{i}\omega/\sigma\right)\left(k_0^2 - \mathrm{i}\omega\right)}{k_0^4 + \omega^2 + 2k_0^2 k_{0\perp}^4 (|\psi_L|^2 + |\psi_R|^2)} (RaK)\psi_L + k_0^2 \left(k_0^2 + \mathrm{i}\omega/\sigma\right)^2 \psi_L = 0, \tag{5.18}$$

$$-\hat{\Omega}_3^2 \mathrm{D}^2\psi_R - \frac{k_{0\perp}^2 \left(k_0^2 + \mathrm{i}\omega/\sigma\right)\left(k_0^2 - \mathrm{i}\omega\right)}{k_0^4 + \omega^2 + 2k_0^2 k_{0\perp}^4 (|\psi_L|^2 + |\psi_R|^2)} (RaK)\psi_R + k_0^2 \left(k_0^2 + \mathrm{i}\omega/\sigma\right)^2 \psi_R = 0. \tag{5.19}$$

The dominant feedback in the overstable regime is thus the same as in the steady regime, i.e. the deformation of the mean temperature profile.

These coupled nonlinear eigenvalue problems are degenerate as a consequence of the fact that in the rapid rotation limit the leading nonlinearity comes only from the horizontally averaged temperature profile. Indeed, with

$$\psi_L = \frac{\Psi}{(1 + |c|^2)^{1/2}}, \qquad \psi_R = \frac{c\Psi}{(1 + |c|^2)^{1/2}}, \tag{5.20}$$

equations (5.18), (5.19) collapse into a single equation

$$-\hat{\Omega}_3^2 \mathrm{D}^2\Psi - \frac{k_{0\perp}^2 \left(k_0^2 + \mathrm{i}\omega/\sigma\right)\left(k_0^2 - \mathrm{i}\omega\right)}{k_0^4 + \omega^2 + 2k_0^2 k_{0\perp}^4 |\Psi|^2} (RaK)\Psi + k_0^2 \left(k_0^2 + \mathrm{i}\omega/\sigma\right)^2 \Psi = 0, \tag{5.21}$$

with K given by an appropriate modification of (5.17). This equation is to be solved subject to the boundary conditions

$$\Psi(0) = \Psi(1) = 0, \tag{5.22}$$

imposing impermeability of the boundaries. The solution of this problem thus defines a two-parameter family of solutions depending on the complex parameter c; this family includes the travelling waves ($c = 0$) and standing waves ($|c| = 1$) familiar from weakly nonlinear theory (Knobloch & Silber 1990). We solve this complex eigenvalue problem for K and the nonlinear oscillation frequency ω using, once

again, the NRK package. Note that in the limit $\omega \to 0$ this problem reduces to equation (4.26) obtained in the steady case (Bassom & Zhang 1994), and to the $\vartheta = 0$ overstable case examined by Julien & Knobloch (1997), providing a valuable check on the calculations.

The SW and TW solutions constructed from the solution of (5.21), (5.22) have two interesting properties, both of which are a direct consequence of the complex nature of the eigenvalue problem. In contrast to the linear SW eigenfunction for stress-free boundaries familiar from linear theory, there is no instant in time during which the nonlinear SW oscillation comes to a complete rest: the kinetic energy of the nonlinear oscillation is at all times positive. As shown in figure 9 this is so for both NS and EW standing waves. Similarly, we find that in a nonlinear TW the boundaries between adjacent cells are bowed out, again in contrast to linear theory with stress-free boundaries. We illustrate this behaviour in figure 10. Qualitatively similar results obtain even in linear theory when no-slip boundary conditions are employed (Knobloch & Moore 1988). The corresponding time- and small-scale averaged Nusselt number K is shown in figure 11(a). This quantity is the same for both SW and TW (cf. Julien & Knobloch 1997), although it depends both on orientation and latitude. As in the steady state the Nusselt number increases rapidly with the applied Rayleigh number before settling down to a slower growth rate. For the case shown in figure 11(a) oscillatory convection transports more heat that steady convection. Note that for a TW the Nusselt number is time-independent to all orders in $E^{1/3}$; this is not so for SW, for which the Nusselt number oscillates with frequency 2ω and $O(E^{1/3})$ amplitude about K. The corresponding nonlinear eigenfrequency is shown in figure 11(b). In all cases the frequency increases monotonically from its onset value as Ra increases, but the increase is small, although it is higher for NS rolls than for EW ones. Moreover, with increasing Ra the NS and EW frequency differences appear to approach one another and saturate. All of these results are for $\sigma = 0.4574$, the value of the Prandtl number maximizing the oscillation frequency at onset.

Note, finally, that equations (5.21), (5.22) can be used to recover the results of linear theory simply by setting $\mathrm{D}\overline{T}_0 = -1$. Moreover, at fixed Ra the wavenumber $k_{0\perp} = k_{0TB}$ provides an upper limit on the wavenumbers for which oscillations (linear and nonlinear) are present (cf. figure 4). For $k_{0\perp} \geqslant k_{0TB}$ the only nonlinear solutions are the steady states, cf. Julien & Knobloch (1997). Moreover, for $k_{0\perp} \leqslant k_{0TB}$, the nonlinear oscillation frequency ω_0 does not change appreciably from (3.19).

6. Heat fluxes and mean flows

Using the nonlinear results of the preceding sections we can now calculate the transport properties of both steady and oscillatory convection at arbitrary latitude. We first obtain local results, using an overbar to indicate averages over the small scales x, y and z. Global quantities can be obtained by integrating the local quantities across the fluid layer. We summarize here the results for steady convection; the corresponding results for oscillatory convection are relegated to Appendix B. In terms of the unscaled (u, v, w) the vertical and horizontal heat fluxes are

$$N = -\mathrm{D}\overline{T}_0 + \overline{w\theta} = -\mathrm{D}\overline{T}_0 + k_{0\perp}^2 \overline{\psi_0 \theta_0} + O(E^{1/3}) = K + O(E^{1/3}). \tag{6.1}$$

$$\overline{u\theta} = \overline{(\phi_{0y} + \psi_{0xz})\theta_0} + O(E^{1/3}) = \frac{2k_{0x}k_{0z}k_{0\perp}^2 \mathrm{D}\overline{T}_0}{k_0^2}|\psi_S|^2 + O(E^{1/3}), \tag{6.2}$$

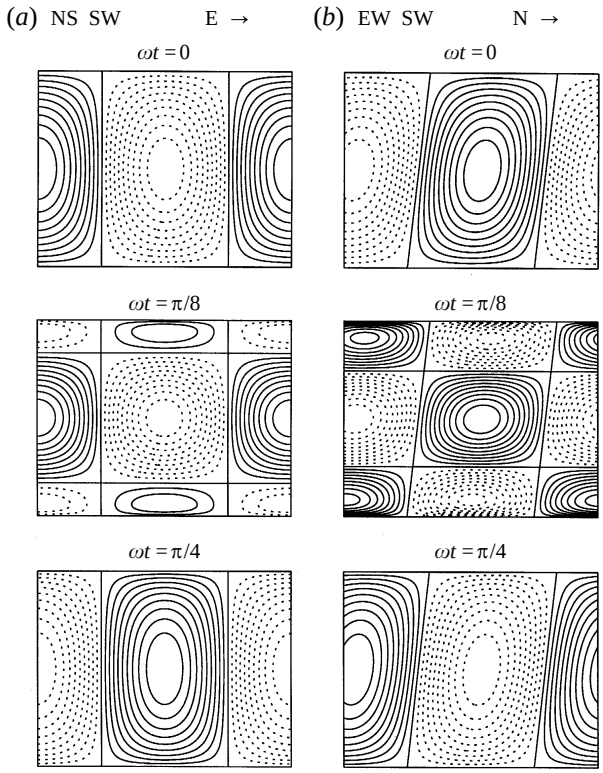

FIGURE 9. Instantaneous streamlines in a nonlinear standing wave at $\vartheta = 45°$ oriented in (*a*) the NS and (*b*) the EW directions showing the reversal phase of an oscillation. The full period is 2π. Maximum amplitude of ψ in successive panels is 197.2, 18.5, 170.9 and 208.8, 80.8, 115.0, respectively. The parameters are $Ra\ E^{4/3} = 100$, $k_{0\perp}\ E^{1/3} = 0.79$ (NS), 0.56 (EW), $\omega\ E^{1/3} = 0.76$ and $\sigma = 0.4574$. The (weak) countercells appear near minima in the kinetic energy. Solid (dotted) lines indicate clockwise (counterclockwise) motion.

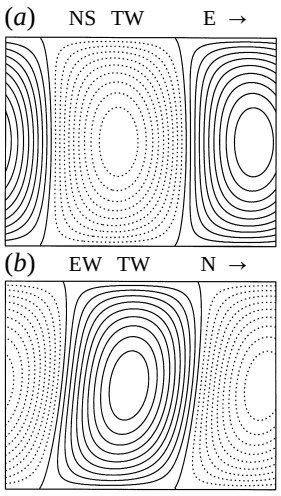

FIGURE 10. Instantaneous streamlines in (*a*) a south-travelling wave and (*b*) a west-travelling wave for the parameter values used in figure 9. The waves lag in the middle; their amplitudes ψ are (*a*) 130.5, (*b*) 116.5.

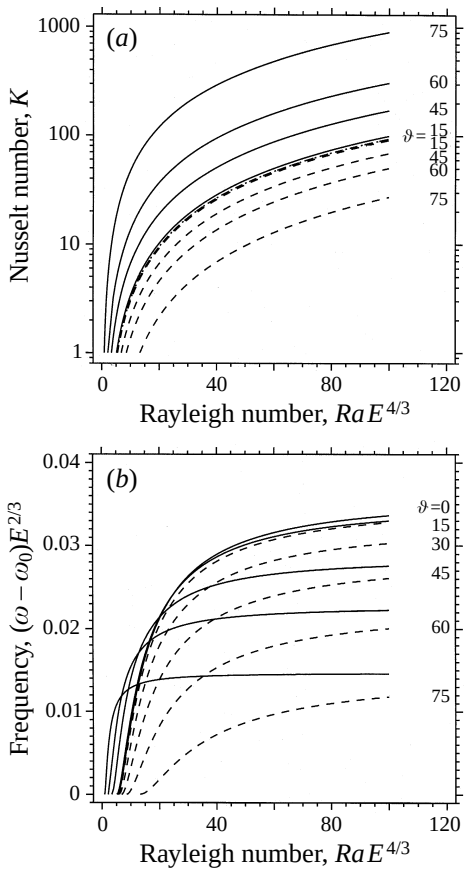

FIGURE 11. (*a*) The Nusselt number K and (*b*) the oscillation frequency ω as functions of the (scaled) Rayleigh number $Ra\ E^{4/3}$ for $\sigma = 0.4547$ and several different colatitudes ϑ. Solid (dashed) lines indicate results for NS (EW) oriented rolls. The frequencies are presented relative to their onset values $\omega_{\rm crit} \equiv \omega_0$, cf. equation (3.22).

$$\overline{v\theta} = \overline{(-\phi_{0x} + \psi_{0yz})\theta_0} + O(E^{1/3}) = \frac{2k_{0y}k_{0z}k_{0\perp}^2 \mathrm{D}\overline{T}_0}{k_0^2}|\psi_S|^2 + O(E^{1/3}), \tag{6.3}$$

while the six independent components of the Reynolds stress tensor are

$$\begin{aligned}\overline{uv} &= E^{-2/3}\overline{(\phi_{0y} + \psi_{0xz})(-\phi_{0x} + \psi_{0yz})} + O(E^{-1/3}) \\ &= 2E^{-2/3}k_{0x}k_{0y}\left[-\left(\frac{\hat{\Omega}_3}{k_0^2}\right)^2 |\mathrm{D}\psi_S|^2 + k_{0z}^2|\psi_S|^2\right] + O(E^{-1/3}),\end{aligned} \tag{6.4}$$

$$\overline{uw} = -E^{-2/3}\overline{(\phi_{0y} + \psi_{0xz})\nabla_\perp^2\psi_0} + O(E^{-1/3}) = -2E^{-2/3}k_{0x}k_{0z}k_{0\perp}^2|\psi_S|^2 + O(E^{-1/3}), \tag{6.5}$$

$$\overline{vw} = -E^{-2/3}\overline{(-\phi_{0x} + \psi_{0yz})\nabla_\perp^2\psi_0} + O(E^{-1/3}) = -2E^{-2/3}k_{0y}k_{0z}k_{0\perp}^2|\psi_S|^2 + O(E^{-1/3}), \tag{6.6}$$

$$\overline{u^2} = 2E^{-2/3}\left[\frac{k_{0y}^2\hat{\Omega}_3^2}{k_0^4}|\mathrm{D}\psi_S|^2 + k_{0x}^2k_{0z}^2|\psi_S|^2\right] + O(E^{-1/3}), \tag{6.7}$$

$$\overline{v^2} = 2E^{-2/3}\left[\frac{k_{0x}^2\hat{\Omega}_3^2}{k_0^4}|\mathrm{D}\psi_S|^2 + k_{0y}^2k_{0z}^2|\psi_S|^2\right] + O(E^{-1/3}), \tag{6.8}$$

$$\overline{w^2} = 2E^{-2/3}k_{0\perp}^4|\psi_S|^2 + O(E^{-1/3}). \tag{6.9}$$

These results imply the following leading-order results, valid at any latitude:

$$\overline{uw} = -\left(\frac{k_{0x}k_{0z}}{k_{0\perp}^2}\right)\overline{w^2}, \qquad \overline{vw} = -\left(\frac{k_{0y}k_{0z}}{k_{0\perp}^2}\right)\overline{w^2}, \tag{6.10}$$

and

$$k_{0x}^2\overline{u^2} - k_{0y}^2\overline{v^2} = \left(\frac{k_{0x}^2 - k_{0y}^2}{k_{0\perp}^2}\right)k_{0z}^2\overline{w^2}, \tag{6.11}$$

$$\overline{uv} = \frac{k_{0x}k_{0y}}{k_{0\perp}^2}\left[-\frac{k_{0y}^2\overline{u^2}}{k_{0y}^2 - k_{0x}^2} + \frac{k_{0x}^2\overline{v^2}}{k_{0y}^2 - k_{0x}^2} + \frac{k_{0z}^2}{k_{0\perp}^2}\overline{w^2}\right]. \tag{6.12}$$

These relations are fully nonlinear results holding in the bulk, and suggest a possible closure scheme for rapidly rotating turbulent convection.

The Reynolds stresses computed above can now be used to determine the mean flows they drive. In steady state these satisfy the equations (again in unscaled variables)

$$-E^{-1}\hat{\Omega}_3\overline{v} = \mathrm{D}^2\overline{u} - \frac{1}{\sigma}\mathrm{D}(\overline{uw}), \tag{6.13}$$

$$E^{-1}\hat{\Omega}_3\overline{u} = \mathrm{D}^2\overline{v} - \frac{1}{\sigma}\mathrm{D}(\overline{vw}). \tag{6.14}$$

Since, generically, $\overline{uw}$, $\overline{vw} = O(E^{-2/3})$ we see immediately that $\overline{u}$, $\overline{v} = O(E^{1/3})$. Thus

$$u = E^{-1/3}(\phi_y + \psi_{xz} + E^{1/3}\mathrm{D}\psi_x) + E^{1/3}\overline{u}, \tag{6.15}$$

$$v = E^{-1/3}(-\phi_x + \psi_{yz} + E^{1/3}\mathrm{D}\psi_y) + E^{1/3}\overline{v}, \tag{6.16}$$

$$w = -E^{-1/3}\nabla_\perp^2\psi. \tag{6.17}$$

It follows that the mean flows are too weak to affect the leading-order nonlinear solutions obtained above, and therefore that the (scaled) mean flows

$$\hat{\Omega}_3\overline{v} = -\frac{2}{\sigma}k_{0x}k_{0z}k_{0\perp}^2\mathrm{D}(|\psi_S|^2) + O(E^{1/3}), \tag{6.18}$$

$$\hat{\Omega}_3\overline{u} = \frac{2}{\sigma}k_{0y}k_{0z}k_{0\perp}^2\mathrm{D}(|\psi_S|^2) + O(E^{1/3}), \tag{6.19}$$

are determined *self-consistently*. In particular for general roll orientation mean flows in both north–south and east–west directions will be generated.

In the following we specialize the above results to the two cases of primary interest: NS rolls and EW rolls. Recall that $(k_{0x}, k_{0y}, k_{0z}) = k_{0\perp}(\cos\chi, \sin\chi, -\sin\chi\tan\vartheta)$. For the NS rolls $\chi = 0$, while for the EW rolls $\chi = \frac{1}{2}\pi$. Thus for the NS rolls $\overline{u\theta}$, $\overline{v\theta}$ are at most $O(E^{1/3})$ while $\overline{uv}$, $\overline{uw}$, $\overline{vw}$, and $\overline{u^2}$ are at most $O(E^{-1/3})$. The dominant components of the stress tensor are

$$\overline{v^2} = 2E^{-2/3}\left(\frac{\cos\vartheta}{k_0}\right)^2|\mathrm{D}\psi_S|^2 + O(E^{-1/3}), \tag{6.20}$$

and

$$\overline{w^2} = 2E^{-2/3}k_{0\perp}^4|\psi_S|^2 + O(E^{-1/3}). \tag{6.21}$$

In fact it is possible to be more precise by calculating the next-order contributions. One then finds that

$$\overline{uv} = -2E^{-1/3}\cos\vartheta\,|\mathrm{D}\psi_S|^2 + O(1) < 0. \tag{6.22}$$

$$\overline{uw} = O(1), \tag{6.23}$$

and

$$\overline{vw} = O(E^{-1/3}). \tag{6.24}$$

Finally

$$\overline{u^2} = 2k_{0\perp}^2|\mathrm{D}\psi_S|^2 + O(E^{1/3}). \tag{6.25}$$

It follows that for NS rolls

$$\frac{\overline{uv}}{(\overline{u^2}\,\overline{v^2})^{1/2}} = -1, \tag{6.26}$$

while

$$\frac{\overline{vw}}{(\overline{v^2}\,\overline{w^2})^{1/2}} = O(E^{1/3}), \qquad \frac{\overline{uw}}{(\overline{u^2}\,\overline{w^2})^{1/2}} = O(E^{1/3}), \tag{6.27}$$

in contrast to the general case in which these quantities are all $O(1)$. We find similarly that

$$\overline{u\theta} = O(E^{2/3}), \qquad \overline{v\theta} = O(E^{1/3}). \tag{6.28}$$

$$\overline{u} = O(E^{2/3}), \qquad \overline{v} = O(E). \tag{6.29}$$

The corresponding results for EW rolls are that $\overline{u\theta}$ is $O(E^{1/3})$ while $\overline{uv}$ and $\overline{uw}$ are both $O(E^{-1/3})$. However

$$\overline{v\theta} = -k_{0\perp}^2\sin 2\vartheta\,|\psi_S|^2\,\mathrm{D}\overline{T}_0, \tag{6.30}$$

a quantity that is always positive. The dominant heat transport is therefore poleward. The dominant components of the stress tensor are

$$\overline{u^2} = 2E^{-2/3}\frac{\cos^4\vartheta}{k_{0\perp}^2}|\mathrm{D}\psi_S|^2 + O(E^{-1/3}), \qquad \overline{v^2} = 2E^{-2/3}k_{0\perp}^4\tan^2\vartheta\,|\psi_S|^2 + O(E^{-1/3}), \tag{6.31}$$

$$\overline{w^2} = 2E^{-2/3}k_{0\perp}^4|\psi_S|^2 + O(E^{-1/3}), \tag{6.32}$$

and

$$\overline{vw} = 2E^{-2/3}k_{0\perp}^4\tan\vartheta\,|\psi_S|^2 + O(E^{-1/3}) > 0. \tag{6.33}$$

Thus

$$\frac{\overline{vw}}{(\overline{v^2}\,\overline{w^2})^{1/2}} = 1 + O(E^{1/3}). \tag{6.34}$$

Moreover,

$$\overline{u} = O(E^{1/3}), \qquad \overline{v} = O(E^{2/3}). \tag{6.35}$$

These results should be compared with those for NS rolls. Specifically EW rolls are much more efficient at driving mean flows than NS rolls, as noted already by Busse (1982). Note also that for both NS and EW rolls advection by the EW mean flow will modify the EW heat flux, while the larger NS heat flux is unaffected at leading order by the corresponding mean flow.

All of the above results are pointwise results at a particular location Z in the layer. In the following we illustrate these results by showing vertical profiles of both the heat flux and Reynolds stress components as functions of the Rayleigh number at $\vartheta = 45^\circ$,

and in integrated form as functions of both Ra and ϑ. Figure 12 summarizes these results for NS rolls. The first set of panels (figure 12*a*) shows the dominant diagonal components of the vertically averaged stress tensor, $\langle\overline{v^2}\rangle$ and $\langle\overline{w^2}\rangle$, as a function of the (scaled) Rayleigh number for several different colatitudes ϑ. Here and hereafter $\langle\cdots\rangle \equiv \int_0^1(\cdots)\,\mathrm{d}Z$. The dotted line indicates the case $\vartheta = 0$. Both quantities are increasing functions of both Ra and ϑ, with $\langle\overline{v^2}\rangle$ increasing more rapidly as a function of Ra than $\langle\overline{w^2}\rangle$, as ϑ increases. The remaining transports all vanish to leading order in $E^{1/3}$ and are omitted. The second set of panels (figure 12*b*) shows the corresponding vertical profiles at midlatitude. NS rolls do not drive an EW mean flow: $\overline{u}(Z) \equiv 0$. These results should be compared with the corresponding ones for EW rolls shown in figure 13. Figure 13(*a*) shows the Rayleigh number and colatitude dependence of $\langle\overline{v\theta}\rangle$, $\langle\overline{vw}\rangle$, $\langle\overline{u^2}\rangle$ and $\langle\overline{v^2}\rangle$; $\langle\overline{w^2}\rangle$ (not shown) resembles $\langle\overline{u^2}\rangle$ in its parameter dependence, with $\langle\overline{u^2}\rangle - \langle\overline{w^2}\rangle$ positive at each Ra and increasing with ϑ. Like the Nusselt number K (see figure 8) both $\langle\overline{u^2}\rangle$ and $\langle\overline{w^2}\rangle$ decrease with ϑ, the latter rapidly so. In contrast the ϑ-dependence of $\langle\overline{vw}\rangle$, $\langle\overline{v\theta}\rangle$ and $\langle\overline{v^2}\rangle$ is non-monotonic, although for the latter two it does become monotonic at sufficiently large Ra; $\langle\overline{vw}\rangle$ is maximum for $\vartheta = 45^\circ$ at all Ra. The vertical profiles at midlatitude of $\overline{u}$, $\overline{v\theta}$, $\overline{u^2}$ and $\overline{v^2}$ are shown in figure 13(*b*) for several values of the Rayleigh number. Note in particular the development of a strong (antisymmetric) shear $\langle\overline{u}\rangle$ in the EW direction, in contrast to the rather uniform NS heat transport associated with it. At this latitude $\overline{v^2} = \overline{w^2} = \overline{vw}$, to leading order.

It is of interest to compare these results with those from three-dimensional numerical simulations of rotating convection carried out by Hathaway & Somerville (1983). These authors consider several different latitudes and rotation rates. In their case (iv), carried out at $\vartheta = 75^\circ$ and $Ta = 10^5$, only the NS rolls are unstable, and Hathaway & Somerville find that

$$\frac{\langle\overline{uv}\rangle}{(\langle\overline{u^2}\rangle\langle\overline{v^2}\rangle)^{1/2}} = -0.80, \tag{6.36}$$

while

$$\frac{\langle\overline{vw}\rangle}{(\langle\overline{v^2}\rangle\langle\overline{w^2}\rangle)^{1/2}} = -0.05, \qquad \frac{\langle\overline{uw}\rangle}{(\langle\overline{u^2}\rangle\langle\overline{w^2}\rangle)^{1/2}} = -0.015. \tag{6.37}$$

Evidently these results are in excellent, even quantitative, agreement with the predictions from our two-dimensional nonlinear results. Moreover, Hathaway & Somerville also find that the EW mean flow is substantially larger than the NS mean flow with both small, while the equatorward heat flux is 3% of the vertical flux. Our prediction that $\langle\overline{v\theta}\rangle = O(E^{1/3})$ is in reasonable agreement with this value. Evidently in cases where the turbulent convection is dominated by a two-dimensional instability its statistical properties are captured very well by the asymptotic results presented here. As expected the agreement is worse for Hathaway & Somerville's case (iii). This case, carried out for the same latitude but $Ta = 10^4$, is further away from the asymptotic limit considered here and is contaminated by the EW rolls which are now unstable as well. Indeed, for this case, Hathaway & Somerville find equatorward transport, while for pure EW rolls we predict poleward heat transport. In fact Julien *et al.* (1997) find poleward heat transport irrespective of the boundary conditions (stress-free or no-slip) once the Rayleigh number is sufficiently large. The qualitative tendencies indicated by these results are to a large extent a consequence of the Coriolis force, rather than viscosity or nonlinearity, as can be seen by comparing them with those obtained by Hathaway *et al.* (1979) in their study of the linear stability problem for

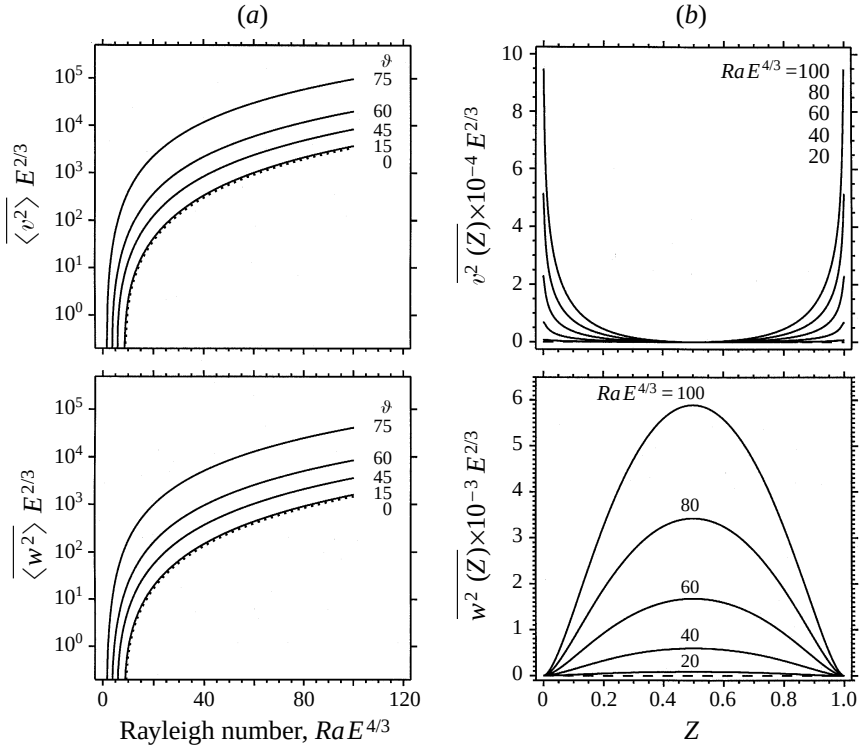

FIGURE 12. (*a*) Non-zero vertically averaged components of the Reynolds stress for steady NS oriented rolls as a function of the (scaled) Rayleigh number at several colatitudes. (*b*) The corresponding vertical profiles at midlatitude for several values of the Rayleigh number. The dotted curves indicate the results for $\vartheta = 0$; the dashed curves indicate those for $Ra = Ra_{\rm crit}$.

ideal fluids, namely $\langle \overline{uw} \rangle < 0$, $\langle \overline{uv} \rangle = 0$, $\langle \overline{u\theta} \rangle = 0$ for NS rolls, and $\langle \overline{v\theta} \rangle > 0$ for EW rolls. In particular Hathaway *et al.* also find poleward heat transport for EW rolls.

The calculation of the transport properties of overstable convection proceeds in a similar manner, except that we must take care to distinguish between the transport properties of standing and travelling waves, which are quite different. The detailed expressions for standing and travelling waves with arbitrary orientation and those oriented in NS and EW directions can be found in Appendix B. The results are summarized in figures 14 and 15. For standing waves the results of Appendix B can be used to show that the identities (6.10)–(6.12) derived for steady convection continue to hold, provided the meaning of the overbar is extended to include an average over the wave period as well. With this notation, for NS SW

$$\frac{\overline{uv}}{(\overline{u^2}\;\overline{v^2})^{1/2}} = -\frac{k_0^2}{(k_0^4 + \omega^2/\sigma^2)^{1/2}} + O(E^{1/3}), \tag{6.38}$$

while

$$\frac{\overline{vw}}{(\overline{v^2}\;\overline{w^2})^{1/2}} = O(E^{1/3}), \qquad \frac{\overline{uw}}{(\overline{u^2}\;\overline{w^2})^{1/2}} = O(E^{1/3}), \tag{6.39}$$

and

$$\overline{u} = O(E^{2/3}), \qquad \overline{v} = O(E). \tag{6.40}$$

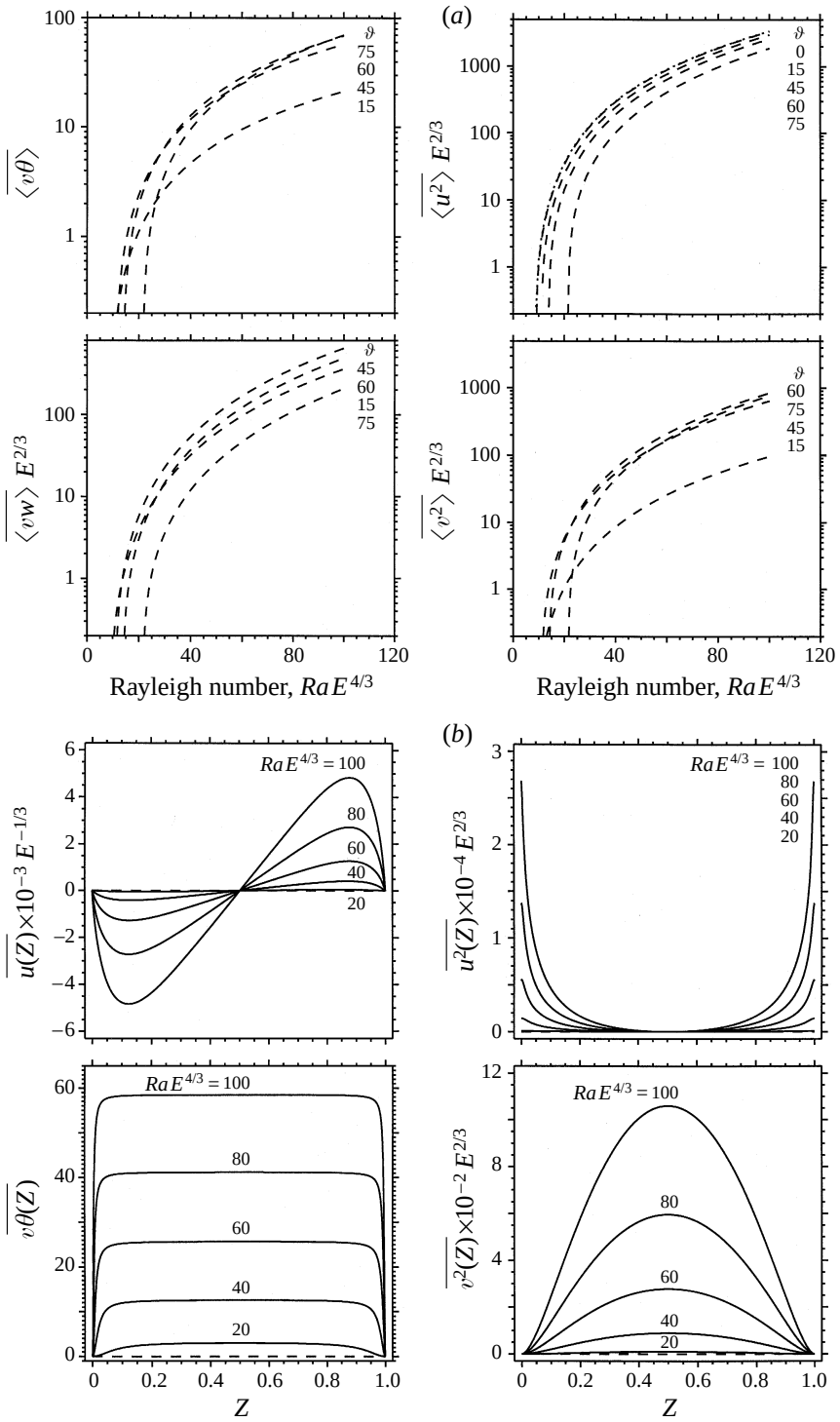

FIGURE 13. As for figure 12 but for EW oriented rolls. The vertically averaged NS heat flux and the midlatitude EW mean flow profile are also shown.

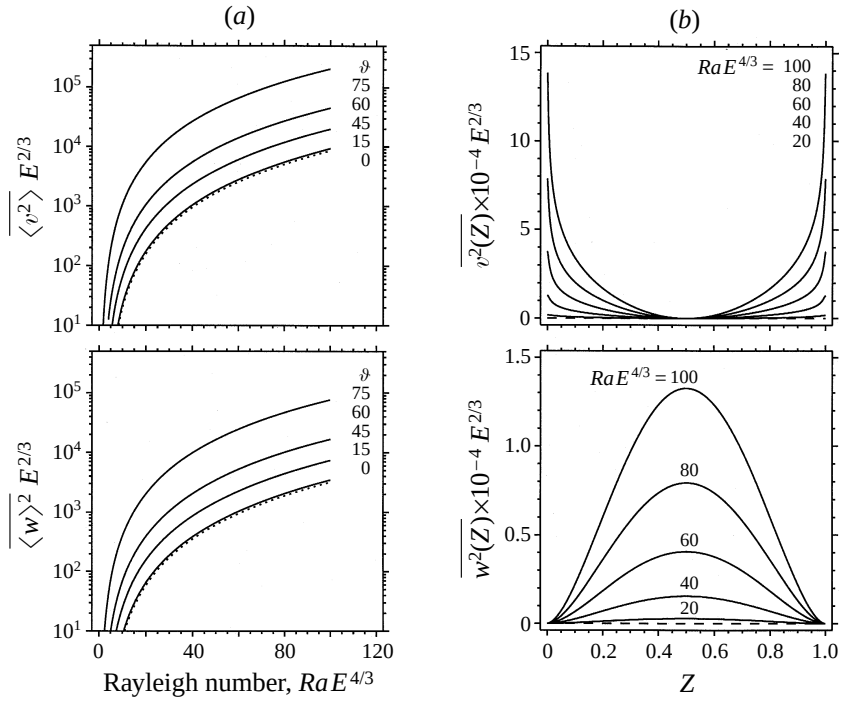

FIGURE 14(*a*, *b*). For caption see facing page.

These results are similar to those for steady rolls except for the fact that the time-dependence of the SW reduces the correlation (6.38), cf. (6.26).

The corresponding results for EW SW are

$$\frac{\overline{vw}}{(\overline{v^2}\,\overline{w^2})^{1/2}} = 1 + O(E^{1/3}). \tag{6.41}$$

$$\frac{\overline{uv}}{(\overline{u^2}\,\overline{v^2})^{1/2}} = O(E^{1/3}), \qquad \frac{\overline{uw}}{(\overline{u^2}\,\overline{w^2})^{1/2}} = O(E^{1/3}), \tag{6.42}$$

while

$$\overline{u} = O(E^{1/3}), \qquad \overline{v} = O(E^{2/3}). \tag{6.43}$$

Moreover $\overline{v\theta} > 0$, i.e. for EW SW the heat flux is poleward.

For left-travelling waves the identity (6.10)–(6.12) no longer applies. Instead we have (cf. Apendix B) the following general results, valid at leading order for left-travelling waves (LTW) at any latitude:

$$\overline{uv} = \frac{1}{2k_{0x}k_{0y}}\left[-k_{0x}^2\overline{u^2} - k_{0y}^2\overline{v^2} + k_{0z}^2\overline{w^2}\right], \tag{6.44}$$

$$\overline{uw} = \frac{1}{2k_{0x}k_{0z}}\left[-k_{0x}^2\overline{u^2} + k_{0y}^2\overline{v^2} - k_{0z}^2\overline{w^2}\right], \tag{6.45}$$

$$\overline{vw} = \frac{1}{2k_{0y}k_{0z}}\left[k_{0x}^2\overline{u^2} - k_{0y}^2\overline{v^2} - k_{0z}^2\overline{w^2}\right]. \tag{6.46}$$

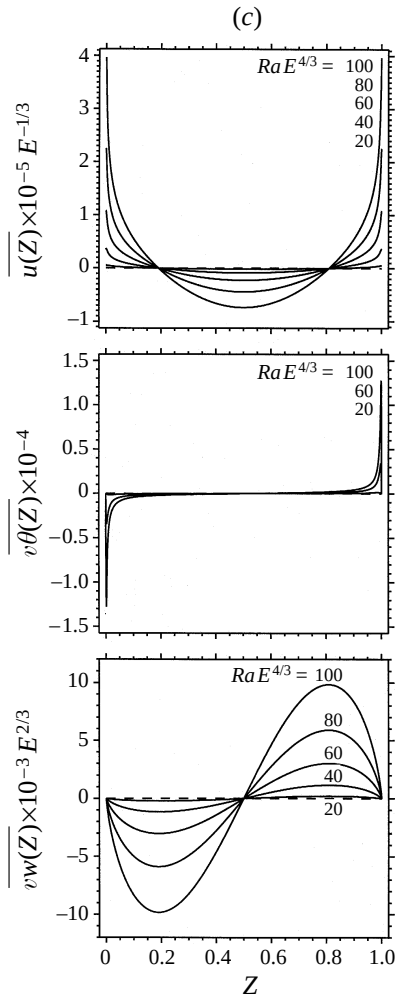

FIGURE 14. (*a*) Non-zero vertically averaged components of the Reynolds stress for NS standing/travelling waves as a function of the (scaled) Rayleigh number at several colatitudes. (*b*) The corresponding vertical profiles at midlatitude for several values of the Rayleigh number. (*c*) Vertical profiles of EW mean flow, NS heat flux and Reynolds stress for left-travelling waves at midlatitude. The dotted curves indicate the results for $\vartheta = 0$; the dashed curves indicate those for $Ra = Ra_{\rm crit}$.

The results in Appendix B also show that for NS LTW

$$\frac{\overline{uv}}{(\overline{u^2}\,\overline{v^2})^{1/2}} = -\frac{k_0^2}{(k_0^4 + \omega^2/\sigma^2)^{1/2}} + O(E^{1/3}), \tag{6.47}$$

$$\frac{\overline{uw}}{(\overline{u^2}\,\overline{w^2})^{1/2}} = O(1), \qquad \frac{\overline{vw}}{(\overline{v^2}\,\overline{w^2})^{1/2}} = O(1), \tag{6.48}$$

while

$$\overline{u} = O(E^{1/3}), \qquad \overline{v} = O(E^{2/3}). \tag{6.49}$$

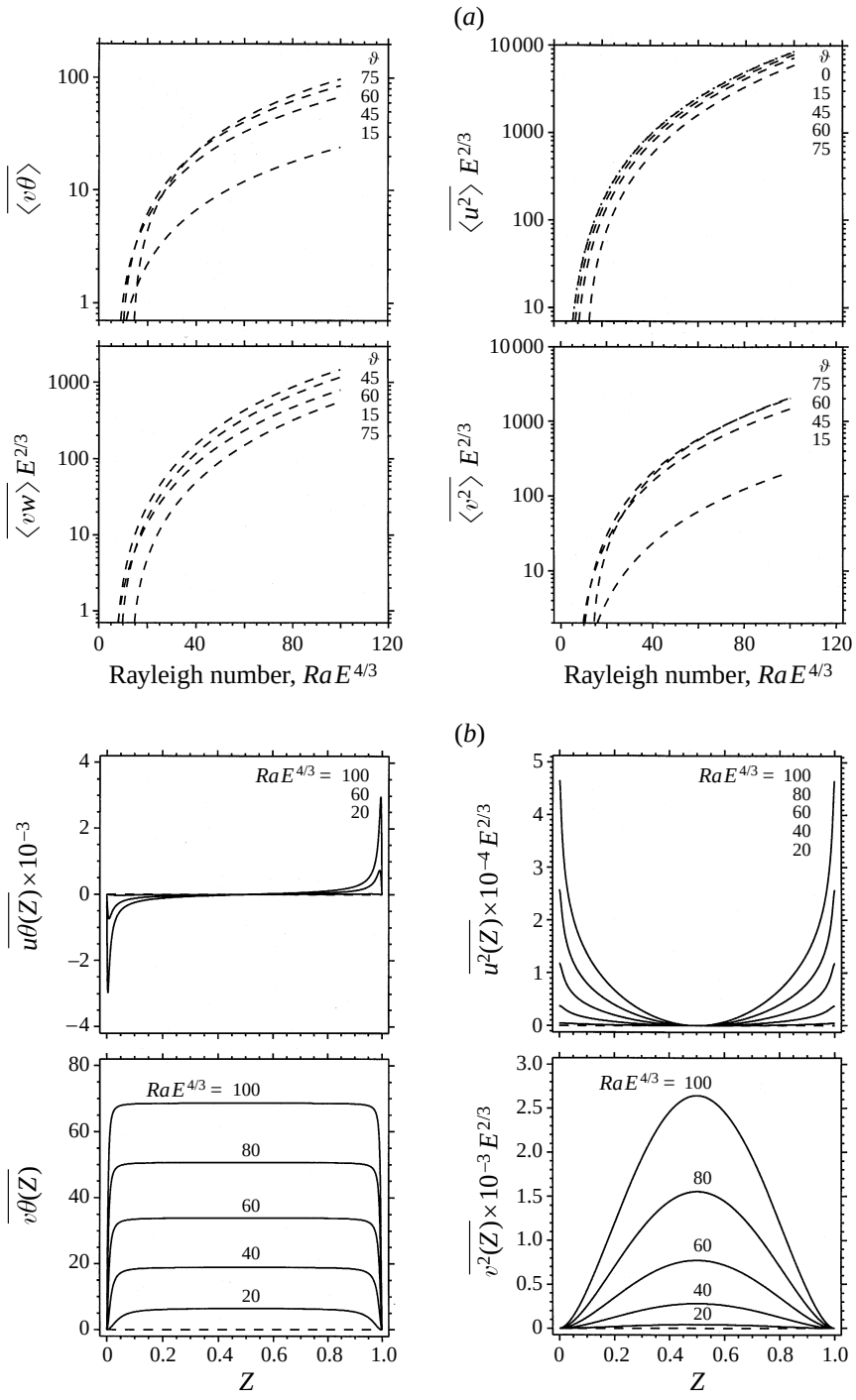

FIGURE 15(*a*, *b*). For caption see facing page.

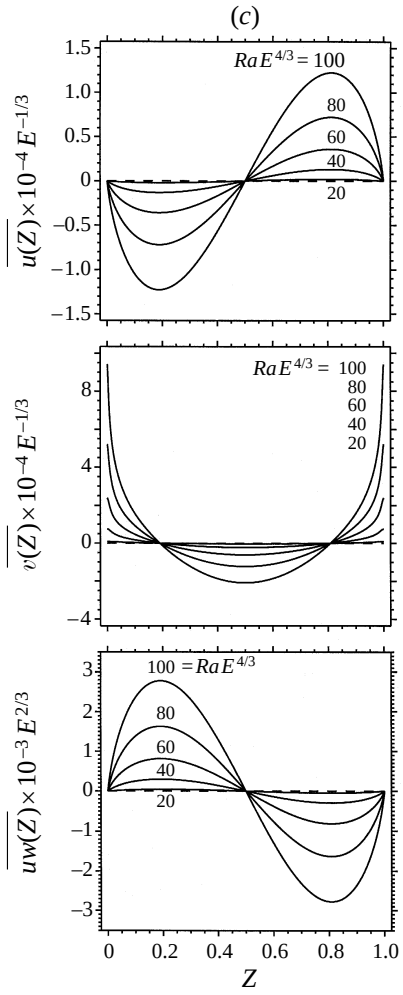

FIGURE 15. As for figure 14 but for EW oriented standing and travelling waves.

In contrast, for EW LTW

$$\frac{\overline{vw}}{(\overline{v^2}\,\overline{w^2})^{1/2}} = 1 + O(E^{1/3}), \qquad \frac{\overline{uv}}{(\overline{u^2}\,\overline{v^2})^{1/2}} = \frac{\overline{uw}}{(\overline{u^2}\,\overline{w^2})^{1/2}} + O(E^{1/3}), \tag{6.50}$$

while

$$\overline{u} = O(E^{1/3}), \qquad \overline{v} = O(E^{1/3}). \tag{6.51}$$

The heat flux $\overline{v\theta}$ is again poleward.

Figure 14 shows detailed results for NS oriented rolls. Since at leading order $\overline{u\theta} = \overline{uv} = \overline{uw} = \overline{u^2} = \langle\overline{v\theta}\rangle = \langle\overline{vw}\rangle = 0$ only $\langle\overline{v^2}\rangle$, $\langle\overline{w^2}\rangle$ and their midlatitude profiles are shown. These results are the *same* for SW and TW, and should be compared with the corresponding ones for steady rolls shown in figure 12. Figure 14(*c*) shows $\overline{u}$, $\overline{v\theta}$ and $\overline{vw}$ for left-travelling waves at $\vartheta = 45°$. For SW these quantities are identically zero (see also the corresponding results for steady rolls); for TW only their vertical averages vanish. Note that the profile of the EW flow $\overline{u}$ is symmetric with respect to midlayer, in contrast to that driven by steady EW rolls which is antisymmetric.

However, both flows have zero mean (i.e. transport zero net mass flux) as required by equations (6.13), (6.14) and the boundary conditions (2.17). Figure 15 shows the corresponding results for EW rolls. Figure 15(*a*) shows $\langle\overline{v\theta}\rangle$, $\langle\overline{vw}\rangle$, $\langle\overline{u^2}\rangle$ and $\langle\overline{v^2}\rangle$ as functions of Ra for several values of ϑ. As in the case of steady rolls $\langle\overline{w^2}\rangle$ (not shown) resembles $\langle\overline{u^2}\rangle$ in its parameter dependence, with $\langle\overline{u^2}\rangle - \langle\overline{w^2}\rangle$ positive at each Ra and increasing with ϑ. Moreover, both $\langle\overline{u^2}\rangle$ and $\langle\overline{w^2}\rangle$ decrease with ϑ, as does the Nusselt number K (see figure 11) while the dependence of $\langle\overline{v\theta}\rangle$, $\langle\overline{vw}\rangle$ and $\langle\overline{v^2}\rangle$ on ϑ depends on Ra. These results are independent of whether the wave is standing or travelling. Figure 15(*b*) shows the midlatitude profiles of $\overline{u\theta}$, $\overline{v\theta}$, $\overline{u^2}$ and $\overline{v^2}$ for several values of the Rayleigh number. The first of these is for a left-travelling wave; for a standing wave it vanishes at leading order. The remaining three quantities are the same for standing and travelling waves. Finally, figure 15(*c*) shows the midlatitude profiles of the mean flows $\overline{u}$, $\overline{v}$ driven by a left-travelling wave as computed from (6.13), (6.14). The profile of $\overline{uw}$ for a left-travelling wave at midlatitude is also shown; for a standing wave this component vanishes to leading order. For travelling waves both $\overline{u}$ and $\overline{v}$ are non-zero; the former flow is odd (antisymmetric) with respect to midlayer, while the latter is even (symmetric). For standing waves $\overline{v} = 0$ at leading order but $\overline{u}$ is the same as for the travelling waves. The NS mean flow driven by EW travelling waves has structure that is very similar to that of the EW flow driven by NS travelling waves (figure 14*c*).

It is instructive to compare the above results with the corresponding ones for steady convection. In general the results for standing waves are similar in order of magnitude to those for steady convection, but with various components of both the heat flux and the stress tensor reduced by the time-dependence. For travelling waves, however, the results are quite different. The larger Reynolds stresses and hence the mean flows driven by them found for this case are a consequence of the phase differences between the various velocity components that are the hallmark of travelling waves. In all cases the wall-layer corrections needed in order that the two-dimensional solutions satisfy the boundary conditions (2.17) imply corresponding corrections to the heat fluxes and Reynolds stresses. The latter result in boundary layer corrections to the mean flows. These introduce Ekman-like spirals into the hodographs of $\overline{u},\overline{v}$ (not shown). This spiralling persists into the bulk for travelling waves but is absent for steady rolls and standing waves, for which equations (6.18), (6.19) imply that the vector direction of the mean flow is constant, given by $\tan^{-1}(k_{0x}/k_{0y})$.

7. Conclusions

In this paper we have shown that fully nonlinear two-dimensional convection on an f-plane is accessible to an asymptotic analysis in powers of the Ekman number. We have discussed in detail the predictions arising from this analysis for the transport properties of such convection as functions of both latitude and roll orientation, and compared the results obtained for steady convection with those for overstable convection in the form of both standing and travelling waves. The analysis started with the observation that unless the rolls are oriented in the north-south direction the critical eigenfunction at onset will have small-scale structure in the vertical. The appearance of this small scale is an immediate consequence of the Taylor–Proudman constraint, and necessitates the use of a two-scale analysis in the vertical direction. Since we examined only states that were periodic in the horizontal we did not employ a two-scale expansion in the horizontal. However, no new difficulties would be

introduced by such a generalization (Julien & Knobloch 1997). In the formulation of the problem we chose to expand the two streamfunctions ϕ and ψ, instead of working with the primitive velocity variables. This approach has a considerable advantage because the incompressibility condition is automatically satisfied. When the primitive variables are used instead this condition introduces substantial difficulties because mixed orders in (u, v, w) have to be combined in order to impose it.

We have shown that the transport properties of the flows, averaged over the small scales (and time if appropriate), can be written down explicitly in terms of the vertical profile of the mean temperature field. A number of simple but useful consequences of these relations, valid at any latitude, could then be derived, even without knowing the mean temperature profile. This profile satisfies a second-order nonlinear eigenvalue problem, with the eigenvalue giving the (time-averaged) Nusselt number (and oscillation frequency if appropriate) for each imposed value of the Rayleigh number. The solution of this problem enabled us to plot the vertical profiles of the mean flows driven by the Reynolds stress, as well as various depth-integrated quantities such as the horizontal heat flux.

Among the general results that follow from this analysis we emphasize the following:

The NS rolls, be they steady or time-dependent, drive weaker mean flows and weaker horizontal heat fluxes than EW oriented rolls, an effect that we attribute to the presence of small vertical scales in the latter.

The mean flows and mean horizontal fluxes are determined self-consistently by the leading-order terms in the expansion.

The EW mean flows are larger than the NS mean flows; the opposite is the case for the heat fluxes.

The transport properties of steady convection and standing wave convection are very similar, with the effectiveness of the latter reduced by its time-dependence.

Travelling waves are the most efficient at momentum and heat transport as a consequence of the phase differences among the various velocity components.

NS travelling waves generate a symmetric zonal mean flow and no meridional mean flow; EW travelling waves generate an antisymmetric zonal mean flow and a symmetric meridional mean flow. For general orientations both components are present and are asymmetric with respect to the midlayer. Such asymmetry in the mean flow profiles has been observed in numerical simulations (Julien *et al.* 1997) and is likely to be due to *parity-breaking* instabilities of steady rolls. These secondary instabilities lead to drifting rolls, i.e. to travelling waves.

All mechanical boundary conditions for the tilted f-plane require Ekman boundary layers, with the exception of NS rolls with stress-free boundaries. These boundary layers are in all instances passive and exhibit spiralling similar to that seen in the classic Ekman layer.

We have compared our results with those of Hathaway & Somerville (1983) obtained from three-dimensional simulations of rotating convection in a $6.0 \times 4.9 \times 1.0$ box with no-slip boundary conditions at top and bottom and periodic ones in the horizontal. While the aspect ratios used by Hathaway & Somerville are not particularly large and their effect on the results unknown we found them to be in remarkably good agreement with our predictions, provided the Taylor number was high ($Ta = 10^5$ was the largest value used) and the flow dominated by a single

roll orientation.† We believe that this comparison provides support for the approach employed here, which shows in turn that several of the correlations measured by Hathaway and Somerville are robust with respect the changes in latitude and boundary conditions at top and bottom (provided these remain symmetric). Unfortunately, similar simulations in the overstable regime are not available, despite their pertinence to astrophysics. However, our results do lead us to speculate that recent helioseismic inferences of spiralling large-scale surface flows (Patron *et al.* 1995) may be evidence of a surface Ekman layer. Such spirals are also observed in numerical simulations of turbulent convection on a tilted f-plane (Brummell *et al.* 1998; Julien *et al.* 1997). Furthermore, our scalings for the transport of momentum and heat fluxes imply that it is unlikely that the f-plane mechanism for generating large-scale mean flows will produce amplitudes comparable to those of convection (such as those observed on the giant planets (Busse 1994)). Alternate mechanisms, such as the inclusion of the β-effect, must be considered (Brummell & Hart 1993).

We believe that the appearance of the small scale in the vertical whenever the roll orientation departs substantially from the NS direction (as it certainly does in the turbulent regime) has substantial implications for mixing length theories of rotating turbulent convection and will report on this aspect of the problem in a future publication.

It remains to comment on the stability of our solutions. Since all the solutions studied here bifurcate supercritically we know that they are stable near onset with respect to perturbations of the same form. Thus when steady convection is the preferred mode of convection (cf. figure 4) we expect our results for steady convection to apply. For low Prandtl numbers overstable convection is preferred and steady convection is unstable, at least near onset. Both travelling and standing waves set in simultanously at onset. Of these we know (cf. Clune & Knobloch 1993; Julien & Knobloch 1997) that travelling waves are preferred in the large-rotation limit when $\vartheta = 0$. As explained in Julien & Knobloch (1997), the generalization of this result to other latitudes requires the consideration of three timescales and is beyond the scope of this paper. However, at such latitudes the NS rolls will be the ones that are stable near onset; with increasing Rayleigh number other orientations come in, modifying the predictions for the NS orientations. For such Rayleigh numbers we expect that our transport results provide upper (EW) and lower (NS) bounds on the actual transports.

This article represents research partially carried out while the first author was an Advanced Study Postdoctoral Fellow at HAO, NCAR and the second author was a Visiting Fellow at JILA, University of Colorado. It was partially supported by the Department of Energy under grant DE-FG03-95ER-25251 and the National Science Foundation under grant DMS-9703684. NCAR is sponsored by the National Science Foundation. The authors wish to thank T. Clune for confirming our linear stability results and to D. Gough, S. Tobias and J. Werne for helpful discussions.

Appendix A. Boundary layer analysis

As already indicated the nonlinear solution obtained in §4 represents the solution in the bulk of the fluid. To satisfy the boundary conditions imposed at the walls boundary layers are necessary. This is so for both stress-free and no-slip boundary conditions. We show here that these boundary layers are passive for the two-dimensional states of interest in the present paper and describe their structure.

† Simulations by Julien *et al.* (1996) have shown that the aspect ratio plays a diminished role in the limit of large rotation.

We begin with equations (2.7)–(2.9). In the boundary layer the leading-order balance is between the (viscous) dissipation and the Coriolis force. The necessary scaling for the vertical extent of the wall layer is given by $z \sim E^{1/2}$. For matching to the bulk solution we retain the outer scalings for the horizontal coordinates and the Rayleigh number. Thus we take

$$\partial_x, \partial_y = E^{-1/3}(\partial_{x'}, \partial_{y'}), \qquad \partial_z = E^{-1/2}\partial_{z'}, \qquad \partial_t = E^{1/3}\partial_{t'}, \qquad Ra = E^{-4/3}Ra', \quad (A\,1)$$

and scale the velocity and temperature fields as follows:

$$\phi = E\phi', \qquad \psi = E^{3/2}\psi', \qquad \theta = E^{1/3}\theta'. \quad (A\,2)$$

These scalings should be compared with the bulk scalings (3.4), (4.2). Equation (2.9) thus becomes

$$-E^{1/2}\partial_z \overline{T}_0 \nabla_\perp^2 \psi = \mathrm{D}^2\theta, \quad (A\,3)$$

where $\mathrm{D} \equiv \partial_z$. Since the mean temperature gradient in the boundary layer is of order one (the layer is thin compared to the thermal boundary layer when rotation is large) this equation shows that $\theta = O(E^{1/2})$ and hence that it decouples from the ϕ, ψ equations. In the boundary layers the temperature therefore plays a passive role. To leading order (2.7), (2.8) become, after dropping primes,

$$-\hat{\Omega}_3 \nabla_\perp^2 \mathrm{D}\psi = \mathrm{D}^2\nabla_\perp^2\phi, \quad (A\,4)$$

$$\hat{\Omega}_3 \nabla_\perp^2 \mathrm{D}\phi + \frac{1}{\sigma}\hat{N}_\psi(\phi,\psi) = \mathrm{D}^4\nabla_\perp^2\psi. \quad (A\,5)$$

Note that these equations are time-independent but nonlinear. However, for the two-dimensional solutions of interest here, the nonlinear term

$$\begin{aligned}\hat{N}_\psi = &-\mathrm{D}^2\left\{J[\phi,\mathrm{D}^2\psi] + J[\mathrm{D}\phi,\mathrm{D}\psi] - \nabla_\perp\phi\cdot\nabla_\perp(\mathrm{D}\phi) - \nabla_\perp(\mathrm{D}\psi)\cdot\nabla_\perp(\mathrm{D}^2\psi)\right\}\\ &-\mathrm{D}\left\{J[\mathrm{D}\psi,\mathrm{D}^2\phi] - J[\phi,\mathrm{D}^3\psi] - 2J[\mathrm{D}\phi,\mathrm{D}^2\psi] + \nabla_\perp\phi\cdot\nabla_\perp(\mathrm{D}^2\phi)\right.\\ &\left.+\nabla_\perp(\mathrm{D}\psi)\cdot\nabla_\perp(\mathrm{D}^3\psi) + |\nabla_\perp(\mathrm{D}\phi)|^2 + |\nabla_\perp(\mathrm{D}^2\psi)|^2\right\}, \end{aligned} \quad (A\,6)$$

vanishes identically! It follows that the boundary layers are described by *linear* equations. These equations are in fact identical to those describing these layers in the linear theory:

$$-\hat{\Omega}_3\mathrm{D}\psi = \mathrm{D}^2\phi, \qquad \hat{\Omega}_3\mathrm{D}\phi = \mathrm{D}^4\psi. \quad (A\,7)$$

The solution to these equations must be matched to the bulk solutions obtained previously. This matching is carried out here for the oscillatory case; the steady case is obtained on setting the frequency to zero. For this purpose we recall that the outer convective solution is given by

$$\psi = E^{4/3}\left(\left[\psi_L(Z)\mathrm{e}^{\mathrm{i}k_z E^{-1/3}Z}\mathrm{e}^{\mathrm{i}\delta_L} + \psi_R(Z)\mathrm{e}^{-\mathrm{i}k_z E^{-1/3}Z}\mathrm{e}^{\mathrm{i}\delta_R} + \mathrm{c.c.}\right] + E^{1/3}\psi_{1/3} + \cdots\right), \quad (A\,8)$$

$$\phi = E\left(\left[\phi_L(Z)\mathrm{e}^{\mathrm{i}k_z E^{-1/3}Z}\mathrm{e}^{\mathrm{i}\delta_L} + \phi_R(Z)\mathrm{e}^{-\mathrm{i}k_z E^{-1/3}Z}\mathrm{e}^{\mathrm{i}\delta_R} + \mathrm{c.c.}\right] + E^{1/3}\phi_{1/3} + \cdots\right), \quad (A\,9)$$

where $\delta_{L,R} = \omega t \pm \boldsymbol{k}_{0\perp}\cdot\boldsymbol{x}$ and $\phi_{L,R}(Z) = [\hat{\Omega}_3/(k_0^2 + i\omega/\sigma)]\mathrm{D}\psi_{L,R}(Z)$. In terms of the wall scale z' it follows that for a rigid boundary at $Z = z' = 0$,

$$\psi(0) = E^{4/3}\left(0 + E^{1/3}\psi_{1/3} + \cdots\right), \quad (A\,10)$$

$$\mathrm{D}\psi(0) = E^{4/3}\left(\frac{E^{1/2}}{(1+|c|^2)^{1/2}}\left[\left(\mathrm{e}^{\mathrm{i}\delta_L} + c\mathrm{e}^{\mathrm{i}\delta_R}\right)\mathrm{D}\Psi(0) + \mathrm{c.c.}\right] + E^{1/3}\mathrm{D}\psi_{1/3} + \cdots\right), \quad (A\,11)$$

$$\phi(0) = E\left(\frac{1}{(1+|c|^2)^{1/2}}\left[\left(\mathrm{e}^{\mathrm{i}\delta_L} + c\mathrm{e}^{\mathrm{i}\delta_R}\right)\Phi(0) + \text{c.c.}\right] + E^{1/3}\phi_{1/3} + \cdots\right), \tag{A 12}$$

where $\Phi(0) = [\hat{\Omega}_3/(k_0^2 + \mathrm{i}\omega/\sigma)]\mathrm{D}\Psi(0)$ and Ψ is the reduced amplitude introduced in equation (5.20). TW(SW) solutions are given by $c = 0(1)$ and steady solutions by $c = 0, \omega = 0$. For a stress-free boundary at $Z = z' = 0$,

$$\psi(0) = E^{4/3}\left(0 + E^{1/3}\psi_{1/3} + \cdots\right), \tag{A 13}$$

$$\mathrm{D}^2\psi(0) = E^{4/3}\left(\frac{2E^{2/3}\mathrm{i}k_{0z}}{(1+|c|^2)^{1/2}}\left[\left(\mathrm{e}^{\mathrm{i}\delta_L} - c\mathrm{e}^{\mathrm{i}\delta_R}\right)\mathrm{D}\Psi(0) + \text{c.c.}\right] + E^{1/3}\mathrm{D}^2\psi_{1/3} + \cdots\right), \tag{A 14}$$

$$\mathrm{D}\phi(0) = E\left(\frac{E^{1/6}\mathrm{i}k_{0z}}{(1+|c|^2)^{1/2}}\left[\left(\mathrm{e}^{\mathrm{i}\delta_L} - c\mathrm{e}^{\mathrm{i}\delta_R}\right)\Phi(0) + \text{c.c.}\right] + E^{1/3}\mathrm{D}\phi_{1/3} + \cdots\right), \tag{A 15}$$

To these expressions we must add the wall layer solution in order to satisfy, at leading order, the boundary condition for the rigid case ($\psi = \partial_z\psi = \phi = 0$) or the stress-free case ($\psi = \partial_z^2\psi = \partial_z\phi = 0$). In terms of the fields scaled according to the outer scaling the boundary layer equations are

$$(\mathrm{D}^4 + \hat{\Omega}_3^2)\psi_E = 0, \qquad E^{1/6}\hat{\Omega}_3\phi_E = \mathrm{D}^3\psi_E, \tag{A 16}$$

with inessential constants of integration omitted. For impenetrable boundaries, $\psi_E(0) = 0$, the boundary layer solution that decays away from the wall takes the form (dropping the prime)

$$\psi_E = A\left(\mathrm{e}^{-\lambda z} - 1\right) + B\left(\mathrm{e}^{-\lambda^* z} - 1\right) + \text{c.c.}, \tag{A 17}$$

$$E^{1/6}\phi_E = -\mathrm{i}\lambda A\mathrm{e}^{-\lambda z} + \mathrm{i}\lambda^* B\mathrm{e}^{-\lambda^* z} + \text{c.c.}, \tag{A 18}$$

with $\lambda = (\mathrm{i}\hat{\Omega}_3)^{1/2}$. No boundary layer contribution θ_E is required. For a rigid boundary the boundary conditions are

$$\partial_z\psi_E(0) = -\frac{E^{1/2}}{(1+c^2)^{1/2}}\left(\mathrm{e}^{\mathrm{i}\delta_L} + c\mathrm{e}^{\mathrm{i}\delta_R}\right)\mathrm{D}\Psi(0), \tag{A 19}$$

$$\partial_{zzz}\psi_E(0) = -\frac{E^{1/6}}{(1+c^2)^{1/2}}\hat{\Omega}_3\left(\mathrm{e}^{\mathrm{i}\delta_L} + c\mathrm{e}^{\mathrm{i}\delta_R}\right)\Phi(0), \tag{A 20}$$

and hence the boundary layer solution is specified by

$$A = -\frac{H}{2\hat{\Omega}_3}\left(\frac{\mathrm{i}\hat{\Omega}_3}{k_0^2 + \mathrm{i}\omega/\sigma}E^{1/6} - E^{1/2}\right)\lambda^*\mathrm{D}\Psi(0), \tag{A 21}$$

$$B = \frac{H}{2\hat{\Omega}_3}\left(\frac{\mathrm{i}\hat{\Omega}_3}{k_0^2 + \mathrm{i}\omega/\sigma}E^{1/6} + E^{1/2}\right)\lambda\mathrm{D}\Psi(0), \tag{A 22}$$

with

$$H = \frac{\mathrm{e}^{\mathrm{i}\delta_L} + c\mathrm{e}^{\mathrm{i}\delta_R}}{(1+|c|^2)^{1/2}}. \tag{A 23}$$

We thus find that the magnitude of the Ekman pumping is given by $W_E = k_{0\perp}^2\psi_E(z \to \infty) \sim O(E^{1/6})$. Similarly, for a stress-free boundary

$$\partial_z^2\psi_E(0) = -\frac{2E^{2/3}ik_{0z}}{(1+c^2)^{1/2}}\left(\mathrm{e}^{\mathrm{i}\delta_L} - c\mathrm{e}^{\mathrm{i}\delta_R}\right)\mathrm{D}\Psi(0), \tag{A 24}$$

$$\partial_z^4 \psi_E(0) = -\frac{E^{1/3} \mathrm{i} k_{0z}}{(1+c^2)^{1/2}} \hat{\Omega}_3 \left(\mathrm{e}^{\mathrm{i}\delta_L} - c\mathrm{e}^{\mathrm{i}\delta_R} \right) \Phi(0). \tag{A 25}$$

The solution is given by

$$A = \frac{H}{2\hat{\Omega}_3} \left(\frac{\mathrm{i}\hat{\Omega}_3}{k_0^2 + \mathrm{i}\omega/\sigma} E^{1/3} - 2E^{2/3} \right) k_{0z} \mathrm{D}\Psi(0), \tag{A 26}$$

$$B = \frac{H}{2\hat{\Omega}_3} \left(\frac{\mathrm{i}\hat{\Omega}_3}{k_0^2 + \mathrm{i}\omega/\sigma} E^{1/3} + 2E^{2/3} \right) k_{0z} \mathrm{D}\Psi(0), \tag{A 27}$$

$$H = \frac{\mathrm{i}(\mathrm{e}^{\mathrm{i}\delta_L} - c\mathrm{e}^{\mathrm{i}\delta_R})}{(1+|c|^2)^{1/2}}. \tag{A 28}$$

Thus with the exception of NS rolls (where $k_{0z} = 0$) Ekman layers exist for stress-free boundaries. The associated pumping is smaller than that experienced in the presence of a no-slip boundary with $W_E = k_{0\perp}^2 \psi_E (z \to \infty) \sim O(E^{1/3})$.

Appendix B. Transport properties of overstable convection

In this Appendix we list the results of calculating the leading-order transport properties of overstable convection. As in §6 we first list the generic expressions followed by the leading-order results for NS and EW oriented rolls. In addition we have to distinguish between overstable convection in the form of standing and travelling waves. We are only interested in time-averaged properties and therefore extend the meaning of the overbar to include a time average as well as an average over small scales. The results that follow are written in terms of the following quantities:

$$\alpha = \mathrm{D}\psi_L \psi_L^* - \mathrm{D}\psi_L^* \psi_L - \mathrm{D}\psi_R \psi_R^* + \mathrm{D}\psi_R^* \psi_R, \tag{B 1}$$

and

$$\beta = \mathrm{D}(|\psi_L|^2 - |\psi_R|^2), \qquad \gamma = |\psi_L|^2 + |\psi_R|^2, \qquad \delta = |\mathrm{D}\psi_L|^2 + |\mathrm{D}\psi_R|^2. \tag{B 2}$$

Here the asterisk denotes the complex conjugate. Note that α and β are odd with respect to the midplane, while γ and δ are even (and positive definite). For rolls with arbitrary orientation we have

$$\overline{N} \equiv -\mathrm{D}\overline{T}_0 + \overline{w\theta} = K + O(E^{1/3}). \tag{B 3}$$

$$\overline{u\theta} = -\frac{k_{0y} \hat{\Omega}_3 k_{0\perp}^2 \mathrm{D}\overline{T}_0}{(k_0^4 + \omega^2/\sigma^2)(k_0^4 + \omega^2)} \left[\mathrm{i}\alpha \left(k_0^4 + \frac{\omega^2}{\sigma} \right) - \omega\beta k_0^2 \left(1 - \frac{1}{\sigma} \right) \right] + \frac{2k_{0x} k_{0z} k_{0\perp}^2 k_0^2 \mathrm{D}\overline{T}_0}{k_0^4 + \omega^2} \gamma + O(E^{1/3}), \tag{B 4}$$

$$\overline{v\theta} = \frac{k_{0x} \hat{\Omega}_3 k_{0\perp}^2 \mathrm{D}\overline{T}_0}{(k_0^4 + \omega^2/\sigma^2)(k_0^4 + \omega^2)} \left[\mathrm{i}\alpha \left(k_0^4 + \frac{\omega^2}{\sigma} \right) - \omega\beta k_0^2 \left(1 - \frac{1}{\sigma} \right) \right] + \frac{2k_{0y} k_{0z} k_{0\perp}^2 k_0^2 \mathrm{D}\overline{T}_0}{k_0^4 + \omega^2} \gamma + O(E^{1/3}), \tag{B 5}$$

$$\overline{uv} = E^{-2/3}\left[-2\delta k_{0x}k_{0y}\left(\frac{\hat{\Omega}_3^2}{k_0^4+\omega^2/\sigma^2}\right)\right.$$
$$\left.+2\gamma k_{0x}k_{0y}k_{0z}^2 - \frac{\mathrm{i}(k_{0y}^2-k_{0x}^2)k_{0z}\hat{\Omega}_3}{k_0^4+\omega^2/\sigma^2}\left(\alpha k_0^2 - \frac{\mathrm{i}\omega}{\sigma}\beta\right)\right] + O(E^{-1/3}), \tag{B 6}$$

$$\overline{uw} = E^{-2/3}k_{0\perp}^2\left[\frac{ik_{0y}\hat{\Omega}_3}{k_0^4+\omega^2/\sigma^2}\left(\alpha k_0^2 - \frac{i\omega}{\sigma}\beta\right) - 2\gamma k_{0x}k_{0z}\right] + O(E^{-1/3}), \tag{B 7}$$

$$\overline{vw} = E^{-2/3}k_{0\perp}^2\left[-\frac{ik_{0x}\hat{\Omega}_3}{k_0^4+\omega^2/\sigma^2}\left(\alpha k_0^2 - \frac{\mathrm{i}\omega}{\sigma}\beta\right) - 2\gamma k_{0y}k_{0z}\right] + O(E^{-1/3}), \tag{B 8}$$

$$\overline{u^2} = 2E^{-2/3}\left[\delta k_{0y}^2\left(\frac{\hat{\Omega}_3^2}{k_0^4+\omega^2/\sigma^2}\right) + \gamma k_{0x}^2k_{0z}^2 - \frac{\mathrm{i}k_{0x}k_{0y}k_{0z}\hat{\Omega}_3}{k_0^4+\omega^2/\sigma^2}\left(\alpha k_0^2 - \frac{\mathrm{i}\omega}{\sigma}\beta\right)\right] + O(E^{-1/3}), \tag{B 9}$$

$$\overline{v^2} = 2E^{-2/3}\left[\delta k_{0x}^2\left(\frac{\hat{\Omega}_3^2}{k_0^4+\omega^2/\sigma^2}\right) + \gamma k_{0y}^2k_{0z}^2 + \frac{\mathrm{i}k_{0x}k_{0y}k_{0z}\hat{\Omega}_3}{k_0^4+\omega^2/\sigma^2}\left(\alpha k_0^2 - \frac{\mathrm{i}\omega}{\sigma}\beta\right)\right] + O(E^{-1/3}), \tag{B 10}$$

$$\overline{w^2} = 2E^{-2/3}k_{0\perp}^4\gamma + O(E^{-1/3}). \tag{B 11}$$

These expressions simplify substantially for standing waves for which $\psi_L = \psi_R$ and for (left)-travelling waves for which $\psi_R = 0$. In the special cases of NS and EW oriented rolls many of these leading order expressions vanish. For example, for east-west standing waves for which $\alpha = \beta = k_{0x} = 0$, $\overline{u\theta} = \overline{uv} = \overline{uw} = 0$ to leading order. As in the steady case it is necessary therefore to extend the above results to higher order. We summarize here the results of such calculations, while omitting the detailed steps.

B.1. *Standing waves*

For NS SW we have

$$\overline{u\theta} = O(E^{2/3}), \qquad \overline{v\theta} = O(E^{1/3}), \tag{B 12}$$

$$\overline{uv} = -4E^{-1/3}\left(\frac{k_0^4\hat{\Omega}_3}{k_0^4+\omega^2/\sigma^2}\right)|\mathrm{D}\psi_L|^2 + O(1), \tag{B 13}$$

$$\overline{uw} = O(1), \qquad \overline{vw} = O(E^{-1/3}), \tag{B 14}$$

$$\overline{u^2} = 4k_0^2|\mathrm{D}\psi_L|^2 + O(E^{1/3}), \tag{B 15}$$

$$\overline{v^2} = 4E^{-2/3}\frac{k_0^2\hat{\Omega}_3^2}{k_0^4+\omega^2/\sigma^2}|\mathrm{D}\psi_L|^2 + O(E^{-1/3}), \tag{B 16}$$

$$\overline{w^2} = 4E^{-2/3}k_0^4|\psi_L|^2 + O(E^{-1/3}), \tag{B 17}$$

while for EW SW

$$\overline{u\theta} = O(E^{1/3}), \qquad \overline{v\theta} = \frac{4k_{0y}^3k_{0z}k_0^2\mathrm{D}\overline{T}_0}{k_0^4+\omega^2}|\psi_L|^2 + O(E^{1/3}), \tag{B 18}$$

$$\overline{uv} = O(E^{-1/3}), \qquad \overline{uw} = O(E^{-1/3}), \tag{B 19}$$

$$\overline{vw} = -4E^{-2/3}k_{0y}^3 k_{0z}|\psi_L|^2 + O(E^{-1/3}), \tag{B 20}$$

$$\overline{u^2} = 4E^{-2/3}\frac{k_{0y}^2\hat{\Omega}_3^2}{k_0^4+\omega^2/\sigma^2}|\mathrm{D}\psi_L|^2 + O(E^{-1/3}), \tag{B 21}$$

$$\overline{v^2} = 4E^{-2/3}k_{0y}^2 k_{0z}^2|\psi_L|^2 + O(E^{-1/3}), \qquad \overline{w^2} = 4E^{-2/3}k_{0y}^4|\psi_L|^2 + O(E^{-1/3}). \tag{B 22}$$

B.2. *Travelling waves*

For NS LTW we have

$$\overline{u\theta} = -E^{1/3}\frac{\mathrm{i}k_0^3\mathrm{D}\overline{T}_0}{k_0^4+\omega^2}\left[k_0^2(\mathrm{D}\psi_L\psi_L^* - D\psi_L^*\psi_L) + \mathrm{i}\omega\mathrm{D}(|\psi_L|^2)\right] + O(E^{2/3}), \tag{B 23}$$

$$\begin{aligned}\overline{v\theta} = {}& \frac{k_0^3\hat{\Omega}_3\mathrm{D}\overline{T}_0}{(k_0^4+\omega^2/\sigma^2)(k_0^4+\omega^2)} \\ & \times\left[\mathrm{i}\left(k_0^4+\frac{\omega^2}{\sigma}\right)(\mathrm{D}\psi_L\psi_L^* - \mathrm{D}\psi_L^*\psi_L) - \omega k_0^2\left(1-\frac{1}{\sigma}\right)\mathrm{D}(|\psi_L|^2)\right] + O(E^{1/3}),\end{aligned} \tag{B 24}$$

$$\overline{uw} = -2E^{-1/3}\frac{k_0^4\hat{\Omega}_3}{k_0^4+\omega^2/\sigma^2}|\mathrm{D}\psi_L|^2 + O(1), \tag{B 25}$$

$$\overline{uw} = E^{-1/3}\mathrm{i}k_0^3(\mathrm{D}\psi_L\psi_L^* - \mathrm{D}\psi_L^*\psi_L) + O(1), \tag{B 26}$$

$$\overline{vw} = -E^{-2/3}\frac{\mathrm{i}k_0^3\hat{\Omega}_3}{k_0^4+\omega^2/\sigma^2}\left[k_0^2(\mathrm{D}\psi_L\psi_L^* - \mathrm{D}\psi_L^*\psi_L) - \frac{i\omega}{\sigma}\mathrm{D}(|\psi_L|^2)\right] + O(E^{-1/3}), \tag{B 27}$$

$$\overline{u^2} = 2k_0^2|\mathrm{D}\psi_L|^2 + O(E^{1/3}), \tag{B 28}$$

$$\overline{v^2} = 2E^{-2/3}\frac{k_0^2\hat{\Omega}_3^2}{k_0^4+\omega^2/\sigma^2}|\mathrm{D}\psi_L|^2 + O(E^{-1/3}), \tag{B 29}$$

$$\overline{w^2} = 2E^{-2/3}k_0^4|\psi_L|^2 + O(E^{-1/3}), \tag{B 30}$$

while for EW LTW

$$\begin{aligned}\overline{u\theta} = {}& -\frac{k_{0y}^3\hat{\Omega}_3\mathrm{D}\overline{T}_0}{(k_0^4+\omega^2/\sigma^2)(k_0^4+\omega^2)} \\ & \times\left[\mathrm{i}\left(k_0^4+\frac{\omega^2}{\sigma}\right)(\mathrm{D}\psi_L\psi_L^* - \mathrm{D}\psi_L^*\psi_L) - \omega k_0^2\left(1-\frac{1}{\sigma}\right)\mathrm{D}(|\psi_L|^2)\right] + O(E^{1/3}),\end{aligned} \tag{B 31}$$

$$\overline{v\theta} = \frac{2k_{0y}^3 k_{0z}k_0^2\mathrm{D}\overline{T}_0}{k_0^4+\omega^2}|\psi_L|^2 + O(E^{1/3}), \tag{B 32}$$

$$\overline{uw} = -E^{-2/3}\frac{ik_{0y}^2 k_{0z}\hat{\Omega}_3}{k_0^4+\omega^2/\sigma^2}\left[k_0^2(\mathrm{D}\psi_L\psi_L^* - \mathrm{D}\psi_L^*\psi_L) - \frac{\mathrm{i}\omega}{\sigma}\mathrm{D}(|\psi_L|^2)\right] + O(E^{-1/3}), \tag{B 33}$$

$$\overline{uw} = E^{-2/3}\frac{\mathrm{i}k_{0y}^3\hat{\Omega}_3}{k_0^4+\omega^2/\sigma^2}\left[k_0^2(\mathrm{D}\psi_L\psi_L^* - \mathrm{D}\psi_L^*\psi_L) - \frac{\mathrm{i}\omega}{\sigma}\mathrm{D}(|\psi_L|^2)\right] + O(E^{-1/3}), \tag{B 34}$$

$$\overline{vw} = -2E^{-2/3}k_{0y}^3 k_{0z}|\psi_L|^2 + O(E^{-1/3}), \tag{B 35}$$

$$\overline{u^2} = 2E^{-2/3}\frac{k_{0y}^2\hat{\Omega}_3^2}{k_0^4+\omega^2/\sigma^2}|\mathrm{D}\psi_L|^2 + O(E^{-1/3}), \tag{B 36}$$

$$\overline{v^2} = 2E^{-2/3}k_{0y}^2k_{0z}^2|\psi_L|^2 + O(E^{-1/3}), \tag{B 37}$$

$$\overline{w^2} = 2E^{-2/3}k_{0y}^4|\psi_L|^2 + O(E^{-1/3}). \tag{B 38}$$

REFERENCES

Baker, L. & Spiegel, E. A. 1975 Modal analysis of convection in a rotating fluid. *J. Atmos. Sci.* **32**, 1909–1920.

Bassom, A. P. & Zhang, K. 1994 Strongly nonlinear convection cells in a rapidly rotating fluid layer. *Geophys. Astrophys. Fluid Dyn.* **76**, 223–238.

Brummell, N. H. & Hart, J. E. 1993 High Rayleigh number β-convection. *Geophys. Astrophys. Fluid Dyn.* **68**, 133–150.

Brummell, N. H., Hurlburt, N. E. & Toomre, J. 1996 Turbulent compressible convection with rotation. Part I: Flow structure and evolution. *Astrophys. J.* **473**, 494–513.

Brummell, N. H., Hurlburt, N. E. & Toomre, J. 1998 Turbulent compressible convection with rotation. Part II: Mean flows and differential rotation. *Astrophys. J.*, **493**, 955–969.

Busse, F. H. 1982 Generation of mean flows in a rotating convection layer. *Z. Naturforsch.* **37a**, 752–758.

Busse, F. H. 1994 Convection driven flows and vortices in the major planets. *Chaos* **4**, 123–134.

Cash, J. R. & Singhal, A. 1982 High order method for the numerical solution of two-point boundary value problems. *B.I.T.* **22**, 184–199.

Chandrasekhar, S. 1961 *Hydrodynamic and Hydromagnetic Stability*. Oxford University Press.

Clune, T. & Knobloch, E. 1993 Pattern selection in rotating convection with experimental boundary conditions. *Phys. Rev.* E **47**, 2536–2550

Hathaway, D. H., Gilman, P. A. & Toomre, J. 1979 Convective instability when the temperature gradient and rotation vector are oblique to gravity. I. Fluids without diffusion. *Geophys. Astrophys. Fluid Dyn.* **13**, 289–316.

Hathaway, D. H. & Somerville, R. C. 1983 Three-dimensional simulations of convection in layers with tilted rotation vectors. *J. Fluid Mech.* **126**, 75–89.

Hathaway, D. H., Toomre, J. & Gilman, P. A. 1980 Convective instability when the temperature gradient and rotation vector are oblique to gravity. II. Real fluids with effects of diffusion. *Geophys. Astrophys. Fluid Dyn.* **15**, 7–37.

Henrici, P. 1962 *Discrete Variable Methods in Ordinary Differential Equations*, Wiley and Sons.

Julien, K. & Knobloch, E. 1997 Fully nonlinear oscillatory convection in a rotating layer. *Phys. Fluids* **9**, 1906–1913.

Julien, K., Legg, S., McWilliams, J. & Werne, J. 1996 Rapidly rotating turbulent Rayleigh-Bénard convection. *J. Fluid Mech.* **322**, 243–273.

Julien, K., Legg, S., McWilliams, J. & Werne, J. 1997 Rapidly rotating turbulent convection on a tilted f-plane. Preprint.

Knobloch, E. 1994 Bifurcations in rotating systems. In *Lectures on Solar and Planetary Dynamos* (ed. M. R. E. Proctor & A. D. Gilbert), pp. 331–372. Cambridge University Press.

Knobloch, E. 1996 Symmetry and instability in rotating hydrodynamic and magnetohydrodynamic flows. *Phys. Fluids* **8**, 1446–1454.

Knobloch, E. & Moore, D. R. 1988 Linear stability of experimental Soret convection. *Phys. Rev.* A **37**, 860–870.

Knobloch, E. & Silber, M. 1990 Travelling wave convection in a rotating layer. *Geophys. Astrophys. Fluid Dyn.* **51**, 195–209.

Ohlsen, D. R., Hart, J. E. & Kittelman, S. 1995 Laboratory experiments on rotating turbulent convection. *Am. Met. Soc. Tenth Conf. on Atmospheric and Oceanic Waves and Stability* (*Preprints*), p. 255.

Patron, J., Hill, F., Rhodes jr., E. J., Korzennik, S. G. & Cacciani, A. 1995 Velocity fields within the solar convection zone: evidence from oscillation ring diagram analysis of Mount Wilson dopplergrams. *Astrophys. J.* **455**, 746–757.